Representation of Lake–Atmosphere Interactions and Lake-Effect Snowfall in the Laurentian Great Lakes Basin among HighResMIP Global Climate Models

MICHAEL NOTARO,[a] JENNA JORNS,[b] AND LAURA BRILEY[b]

[a] *Nelson Institute Center for Climatic Research, University of Wisconsin–Madison, Madison, Wisconsin*
[b] *Great Lakes Integrated Sciences and Assessments, University of Michigan, Ann Arbor, Michigan*

(Manuscript received 23 August 2021, in final form 24 January 2022)

ABSTRACT: Credible modeling, tools, and guidance, regarding the changing Laurentian Great Lakes and the climatic impacts, are needed by local decision-makers to inform their management and planning. The present study addresses this need through a model evaluation study of the representation of lake–atmosphere interactions and resulting lake-effect snowfall in the Great Lakes region. Analysis focuses on an extensive ensemble of 74 historical simulations generated by 23 high-resolution global climate models (GCMs) from the High-Resolution Model Intercomparison Project (HighResMIP). The model assessment addresses the modeling treatment of the Great Lakes, the spatial distribution and seasonality of climatological snowfall, the seasonal cycle of lake-surface temperatures and overlake turbulent fluxes, and the lake-effect ratio between upwind and downwind precipitation. A deeper understanding of model performance and biases is achieved by partitioning results between HighResMIP GCMs that are 1) coupled to 1D lake models versus GCMs that exclude lake models, 2) between prescribed-ocean model configurations versus fully coupled configurations, and 3) between deep Lake Superior versus relatively shallow Lake Erie. While the HighResMIP GCMs represent the Great Lakes by a spectrum of approaches that include land grid cells, ocean grid cells (with lake surface temperature and ice cover boundary conditions provided by the Met Office Hadley Center Sea Ice and Sea Surface Temperature Dataset), and 1D lake models, the current investigation demonstrates that none of these rudimentary approaches adequately represent the complex nature of seasonal lake temperature and ice cover evolution and its impact on lake–atmosphere interactions and lake-effect precipitation in the Great Lakes region.

SIGNIFICANCE STATEMENT: The purpose of this study is to evaluate the capability of high-resolution global climate models to simulate lake–atmosphere interactions and lake-effect snowfall in the Great Lakes region, given the critical influence of the lakes on regional climate and vast societal and environmental impacts of lake-effect snowfall. It is determined that the models inadequately represent lake temperatures and ice cover, often leading to insufficient annual snowfall in the lake-effect zones. More advanced, three-dimensional lake models need to be coupled to climate models to support greater credibility in regional lake and climate simulations and future climate projections.

KEYWORDS: Inland seas/lakes; Climate models; Lake effects

1. Introduction

The Laurentian Great Lakes possess vast socioeconomic, cultural, and ecological value. Containing 20% of the world's surface freshwater supply, they provide vital support to the United States' and Canadian economies through impacts on shipping, drinking water, power production, manufacturing, fishing, and recreation (Vaccaro and Read 2011; Sharma et al. 2018; Rau et al. 2020). The Great Lakes influence regional climate due to their substantial depth, spatial extent, effective heat capacity, and thermal inertia; variability as a source of atmospheric moisture; and contrasts in moisture, heat, friction, and radiation compared to adjacent land (Changnon and Jones 1972; Scott and Huff 1997; Notaro et al. 2013a; Sharma et al. 2018). The lakes' relative warmth and resulting low-level convergence support the Great Lakes basin (GLB) as a preferred region of wintertime cyclogenesis (Petterssen and Calabrese 1959; Colucci 1976; Eichenlaub 1979). The lakes' relatively low roughness enhances overlake wind speeds, compared to surrounding land, leading to shoreline convergence and intensified precipitation (George 1940; Lemire 1961; Xiao et al. 2018).

During the cold season, the lakes' ice-free regions supply moisture to the lower atmosphere through synoptic episodes of evaporation (Blanken et al. 2011; Bennington et al. 2014), with heat and moisture fluxes destabilizing and moistening the boundary layer (Changnon and Jones 1972; Bates et al. 1993; Blanken et al. 2011). Lake-induced precipitation peaks during September–March when cloud cover and precipitation are enhanced downwind of the lakes (Niziol et al. 1995; Scott and Huff 1996; Kristovich and Laird 1998), with lake-effect snow most active during December–January (Braham and Dungey 1984; Notaro et al. 2013a). Annual mean snowfall exceeds 250 cm downwind of each lake (often dropping to half that amount about 300–400 km away from lakeshore) (Eichenlaub 1979; Notaro et al. 2013a). Overlake turbulent fluxes and lake-effect precipitation are dampened by February–March as ice cover becomes extensive (Assel 1990; Niziol et al.

Supplemental information related to this paper is available at the Journals Online website: https://doi.org/10.1175/JAS-D-21-0249.s1.

Corresponding Author: Michael Notaro, mnotaro@wisc.edu

DOI: 10.1175/JAS-D-21-0249.1

1995; Gerbush et al. 2008; Brown and Duguay 2010). Lake-effect snowstorms produce vast socioeconomic impacts on transportation, commerce, agriculture, water supply, utilities, tourism, and hydroelectric generation (Changnon 1979; Norton and Bolsenga 1993; Schmidlin 1993; Kunkel et al. 2002). Local decision-makers (e.g., practitioners) rely on credible climate model projections to prepare for these impacts (Barsugli et al. 2013). For GLB coastal communities that experience lake-effect snowstorms, they need reliable climate information to plan for specific impacts and challenges, such as school closures, winter tourism staffing, car accidents, and road closures limiting access to essential services.

Given the importance of lake–atmosphere interactions and pronounced climate change in the GLB (Angel et al. 2018; Wuebbles et al. 2019), there is a need to generate, evaluate, and improve climate modeling for the region. Large lakes and their regional climate influence are often absent or poorly resolved in coarse global climate models (GCMs) (Mallard et al. 2014, 2015; Briley et al. 2017; Sharma et al. 2018). Consequentially, these models struggle to represent lake–atmosphere interactions, resulting in large regional climate biases and diminished confidence in regional climate projections for large lake basins. The Great Lakes' representation across Coupled Model Intercomparison Project (CMIP) GCMs varies broadly among land, wet soil, ocean, or inland lake grid cells, with the most advanced representation based on 1D lake models with inappropriate assumptions for deep lakes (Roeckner et al. 2003; Subin et al. 2012; Briley et al. 2017). According to Briley et al. (2021), most CMIP5 GCMs lack a satisfactory representation of the Great Lakes and their regional climatic impacts, which limits the credibility of their regional climate projections to local practitioners needing this guidance to develop short- and long-term planning decisions. GCMs are typically insufficient tools for simulating lake-effect snowstorms due to their coarse spatial grid spacing, insufficient topographic representation, challenges in simulating mesoscale circulations and convection, and absence of, or underrepresentation of, the Great Lakes (Notaro et al. 2015a). Fundamental gaps in GCMs' modeling capabilities for the GLB limit the capacity to assess likely climate change impacts, thereby increasing societal vulnerability (Sharma et al. 2018).

The application of regional climate models (RCMs) to the Great Lakes region has yielded significant improvements beyond GCMs due to higher spatial resolution to resolve the lakes and due to captured dynamical processes, yet they still struggle with significant climatic and limnological biases due to coupling to oversimplified lake models for representing lake–atmosphere exchanges of water and energy (Sharma et al. 2018). For example, Notaro et al. (2013a, 2015a) evaluated the 25-km Regional Climate Model version 4 (RegCM4) coupled to a 1D energy-balance lake model (Hostetler and Bartlein 1990), which accounts for vertical heat transfer due to eddy diffusion and convective mixing. The model reproduced the broad spatiotemporal features of lake ice and snowfall in the GLB, including the meso-β features (20–200-km spatial scale) of lake-effect snowstorms, which is consistent with prior studies' expectations for models with comparable grid spacing (Hjelmfelt and Braham 1983; Warner and Seaman 1990; Sousounis and Fritsch 1994; Ballentine et al. 1998). RegCM4 produced overly extensive ice cover and excessive lake surface temperature (LST) biases due to neglected lake circulations (Notaro et al. 2013a, 2015a).

The incorporation of simple 1D lake models in climate models facilitates the general representation of important lake ice–atmosphere interactions (Gula and Peltier 2012; Notaro et al. 2013a, 2015a), such as lake ice formation and its inhibition of turbulent fluxes and lake-effect precipitation. However, such models are inappropriate for simulating the dynamic nature of the vast Great Lakes. One-dimensional lake models cannot resolve many key limnological processes that drive observed spatiotemporal variations in LST and ice cover (Xue et al. 2017). Such concerns include the absence of dynamic lake circulations or explicit advective horizontal mixing, lack of ice motion, oversimplified stratification, deficient treatment of eddy diffusivity, instantaneous mixing of instabilities, and neglect of thermal bar formation (Stepanenko et al. 2010; Martynov et al. 2010; Bennington et al. 2014; Mallard et al. 2014, 2015; Sharma et al. 2018). The absence or oversimplification of these dynamic processes often leads to excessive ice cover, anomalously early or absence of stratification, and positive summertime LSTs biases (Bennington et al. 2010, 2014; Notaro et al. 2013a, 2015a; Xiao et al. 2016). These deficiencies diminish the models' credible application by regional climate service providers and practitioners. For example, excessive simulated historical ice cover leads to insufficient historical lake-effect precipitation and persistent ice cover later this century even under climate warming (Notaro et al. 2015a), struggles with lake stratification development and timing hinders a successful reproduction of the Great Lakes' abrupt historical warming (Zhong et al. 2016), and excessively warm summertime LSTs dampen the lakes' stabilizing influence on the atmosphere and lead to erroneous seasonality of lake turbulent fluxes (Notaro et al. 2013b). Modelers sometimes reduce LST biases in 1D lake models by artificially amplifying vertical eddy diffusivity of deep lakes to imitate neglected dynamic circulation and vertical mixing processes (Subin et al. 2012; Martynov et al. 2012; Bennington et al. 2014; Mallard et al. 2015).

The advantages and disadvantages of 1D lake models are outlined by Perroud et al. (2009), Martynov et al. (2010), Stepanenko et al. (2010), and Subin et al. (2012). The types of 1D lake models include simple two-layer models following similarity theory [e.g., Freshwater Lake model (FLake); Mironov et al. 2010], thermal diffusion models that parameterize eddy diffusivity (e.g., Hostetler and Bartlein 1990), and complex turbulence models. FLake reasonably simulates LST and ice cover patterns across diverse lake classifications but struggles with producing seasonal stratification and substantial temperature biases near the bottom of deep lakes (Subin et al. 2012). While the Hostetler lake model simulates reasonable water temperatures for shallow lakes such as Sparkling Lake, Wisconsin, it produces insufficient mixing across deep lakes (Perroud et al. 2009; Martynov et al. 2010; Stepanenko et al. 2010; Subin et al. 2012).

The High-Resolution Model Intercomparison Project (HighResMIP) is composed of the first ensemble of GCMs

TABLE 1. List of HighResMIP models, their output's resolution in the Great Lakes region, their original atmospheric grid (before any interpolation was applied by the modeling groups), and the number of ensemble members analyzed for highresSST-present and hist-1950. Model families: ⊗: CMCC-CM2; •: EC-Earth3P; ∇: ECMWF-IFS; ◆: FGOALS-f3; Ø: HadGEM3-GC31; λ: MPI-ESM1-2; &: MRI-AGCM3-2; π: NICAM16.

Model abbreviation	Full model name	Output local resolution	Original grid/ nominal resolution	highresSST-present	hist-1950
CMCC-CM2-HR4 ⊗	Centro Euro-Mediterraneo sui Cambiamenti Climatici Coupled Climate Model–High Resolution	102 km	192 × 288, 1° × 1°	0	1
CMCC-CM2-VHR4 ⊗	Centro Euro-Mediterraneo sui Cambiamenti Climatici Coupled Climate Model–Very High Resolution	25 km	768 × 1152, 25 km	1	1
CNRM-CM6-1-HR	Centre National de Recherches Météorologiques Coupled Model version (ver.) 6-1–High Resolution; run generated by Centre Europeen de Recherches et de Formation Avancee en Calcul Scientifique	48 km	T359I, 50 km	0	1
EC-Earth3P •	European Consortium Earth System Model 3P; simulations generated by EC-Earth Consortium	67 km	T255, 100 km	1	3
EC-Earth3P-HR •	European Consortium Earth System Model 3P–High Resolution; generated by EC-Earth Consortium	33 km	T511, 50 km	2	3
ECMWF-IFS-LR ∇	European Centre for Medium-Range Weather Forecasts (ECMWF) Integrated Forecasting System–Low Resolution	95 km	Tco199, 50 km	8	8
ECMWF-IFS-MR ∇	ECMWF Integrated Forecasting System–Medium Resolution	95 km	Tco199, 50 km	0	3
ECMWF-IFS-HR ∇	ECMWF Integrated Forecasting System–High Resolution	48 km	Tco399, 25 km	6	6
FGOALS-f3-L ◆	Chinese Academy of Sciences Flexible Global Ocean–Atmosphere–Land System Model–Finite-Volume ver. 3–Low Resolution	105 km	gs1 × 1, 100 km	1	0
FGOALS-f3-H ◆	Chinese Academy of Sciences Flexible Global Ocean–Atmosphere–Land System Model–Finite-Volume ver. 3–High Resolution	24 km	gs1 × 1, 100 km	1	0
GFDL CM4C192	Geophysical Fluid Dynamics Laboratory Coupled Model ver. 4C192	52 km	c192, 100 km	1	1
HadGEM3-GC31-MM Ø	Hadley Centre Global Environment Model ver. 3 Global Coupled Configuration (Config.) 3.1 ver. MM	66 km	N216, 100 km	3	3
HadGEM3-GC31-HM Ø	Hadley Centre Global Environment Model ver. 3 Global Coupled Config. 3.1 ver. HM	27 km	N512, 50 km	3	4
HadGEM3-GC31-HH Ø	Hadley Centre Global Environment Model ver. 3 Global Coupled Config. 3.1 ver. HH	27 km	N512, 50 km	0	1
INM-CM5-H	Institute of Numerical Mathematics Coupled Model ver. 5–High Resolution	54 km	gs2 × 1.5, 100 km	1	1
IPSL-CM6A-ATM-HR	L'Institut Pierre-Simon Laplace Coupled Model ver. 6A Atmosphere-Only–High Resolution	56 km	LMDZ, 50 km	1	0
MPI-ESM1-2-HR λ	Max Planck Institute Earth System Model ver. 1-2–High Resolution	89 km	T127, 100 km	1	1
MPI-ESM1-2-XR λ	Max Planck Institute Earth System Model ver. 1-2–Very High Resolution	44 km	T255, 50 km	1	1
MRI-AGCM3-2-H &	Meteorological Research Institute Atmospheric Global Climate Model ver. 3-2 High Resolution	53 km	TL959, 25 km	1	0
MRI-AGCM3-2-S &	Meteorological Research Institute Atmospheric Global Climate Model ver. 3-2 Super High Resolution	18 km	TL959, 25 km	1	0

TABLE 1. (*Continued*)

Model abbreviation	Full model name	Output local resolution	Original grid/ nominal resolution	highresSST-present	hist-1950
NICAM16-7S π	Nonhydrostatic Icosahedral Atmospheric Model ver. 16-7S; generated by Japan Agency for Marine-Earth Science and Technology (JAMSTEC), Atmosphere and Ocean Research Institute (AORI), National Institute for Environmental Studies (NIES), RIKEN Center for Computational Science (R-CCS)	53 km	56-km icosahedral	1	0
NICAM16-8S π	Nonhydrostatic Icosahedral Atmospheric Model ver. 16-8S; generated by JAMSTEC, AORI, NIES, and R-CCS	27 km	28-km icosahedral	1	0
NICAM16-9S π	Nonhydrostatic Icosahedral Atmospheric Model ver. 16-9S; generated by JAMSTEC, AORI, NIES, and R-CCS	13 km	14-km icosahedral	1	0

with horizontal resolutions approaching that of the current generation of RCMs, made possible by expanded high-performance computing resources (Haarsma et al. 2016). The project's main goal is to assess the potential benefits of enhanced horizontal resolution (without model tuning or altering vertical resolution) on process representation within all climate system components in multimodel ensemble runs (Haarsma et al. 2016). HighResMIP experiments are partitioned into three tiers, focused on applying both prescribed-ocean [prescribed sea surface temperature (SST)] GCMs (AGCMs) and fully coupled models, for comparison of uncoupled and coupled models, during the period of 1950–2050. The target for high resolution in tier 1 is 25–50 km, compared to a mean resolution of CMIP3 and CMIP5 atmospheric models of 250 and 150 km, respectively. Tier 1 experiments are historically forced Atmospheric Model Intercomparison Project (AMIP)-style AGCM runs (only including atmosphere and land components) for 1950–2014, such as the highresSST-present simulations that are forced by daily observed SSTs and sea ice from the 0.25° Met Office Hadley Center Sea Ice and Sea Surface Temperature Dataset version 2 (HadISST2; Rayner et al. 2003; Titchner and Rayner 2014); while HadISST2 contains LST and ice cover over the Great Lakes, some HighResMIP GCMs instead apply HadISST2 values from the Hudson Bay or Atlantic Ocean. Under tier 2, the hist-1950 coupled ocean–atmosphere simulations start from the 1950 initial state under 1950s conditions. Tier 3 consists of future atmosphere-only simulations for 2015–2100, which are not explored here.

The present study addresses the question, "How reliable are HighResMIP simulations of lake–atmosphere interactions and resulting lake-effect snowfall in the GLB?" The effort contributes to the goal of providing more credible future climate projections to inform regional decision-making, planning, and management.

2. Data and methods

a. Model simulations

The multimodel, high-resolution ensemble, HighResMIP, offers an unprecedented opportunity to assess the capability of high-resolution GCMs to accurately represent lake–atmosphere interactions and resulting lake-effect snowstorms. Snowfall flux, precipitation, surface temperature, sensible heat (SH) flux, and latent heat (LH) flux output for 1950–2014 is downloaded from the Earth System Grid Federation (ESGF) from highresSST-present simulations using uncoupled AGCMs and hist-1950 simulations using coupled GCMs. To focus on HighResMIP models with some potential to simulate lake-effect snow processes, data are downloaded only for GCMs that were run at a grid spacing of roughly 100 km or finer, resulting in an ensemble of 74 simulations using 23 GCMs from 12 model families (Table 1). Of the 23 models available for the highresSST-present configuration, only 15 are available for hist-1950. The model configurations applied in the hist-1950 and highresSST-present simulations are outlined in Tables S1 and S2 in the online supplemental material. All data are processed for the Midwest, GLB, and Northeast United States, defined here as 38°–52°N, 96°–72°W. Among the 23 models, the local horizontal grid spacing (after interpolation by some modeling groups) within the Great Lakes region ranges from 13 km in Nonhydrostatic Icosahedral Atmospheric Model version 16-9S (NICAM16-9S) to 105 km in FGOALS-f3-L, with an across-model mean of 53 km (Table 1, Fig. S1). The across-model mean nominal resolution on the original grids is 62 km. For eight model families (Table 1), output is downloaded at multiple grid spacings, such as 53 km in NICAM16-7S, 27 km in NICAM16-8S, and 13 km in NICAM16-9S, for assessing the benefits of enhancing resolution. Some GCMs, including ECMWF-IFS, report results on a coarser grid than the underlying model to dampen features at the smallest nominally resolved scale to maintain numerical stability. IFS applies a cubic octahedral reduced Gaussian grid, with many calculations performed in spectral space rather than gridpoint space and the meteorological fields represented as the sum of spherical harmonics (Malardel et al. 2016).

Among the models, the Great Lakes are typically represented by hundreds to thousands of grid cells, ranging from 0 in IPSL-CM6A-ATM-HR (or 12 in FGOALS-f3-L if only considering GCMs coupled to a lake model) to 1826 in

TABLE 2. Summary of the treatment of the Great Lakes in HighResMIP models, roughly in the order of increasing complexity. The NoLakeMod ensemble consists of IPSL-CM6A-ATM, EC-Earth3P, INM-CM5-H, HadGEM3-GC31, MRI-AGCM, and NICAM16. The LakeMod ensemble consists of ECMWF-IFS, CNRM-CM6, MPI-ESM1-2, GFDL CM4C192, FGOALS, and CMCC-CM2.

HighResMIP Model	Treatment of Great Lakes
IPSL-CM6A-ATM	In the high-resolution version, the atmosphere is not coupled to an ocean model and the Great Lakes are treated as land surface bare soil using a crude land–sea mask in the atmosphere-only highresSST-present runs.
EC-Earth3P	Given the lack of a lake model, the Great Lakes are treated as water surfaces (if <50% land) with LSTs and ice cover provided by HadISST in the atmosphere-only highresSST-present runs vs using extrapolated ocean SST from Hudson Bay in the fully coupled hist-1950 runs.
INM-CM5-H	Given the lack of a lake model, the Great Lakes are treated as ocean points with specified SSTs and sea ice concentration using the HadISST dataset in the atmosphere-only highresSST-present runs, with initial salinity in lakes prescribed as in the ocean. In the coupled hist-1950 run, the initial state of the lakes is prescribed from 1950 and not dependent on HadISST.
HadGEM3-GC31	Given the lack of a lake model, the Great Lakes are treated as ocean points with specified SSTs and sea ice concentration using the HadISST dataset in the atmosphere-only highresSST-present runs and as ocean points controlled by the ocean model in the coupled hist-1950 runs.
MRI-AGCM	Given the lack of a lake model, the Great Lakes are treated as ocean points with specified SSTs and sea ice concentration using the HadISST dataset in the atmosphere-only highresSST-present runs.
NICAM16	Given the lack of a lake model, the Great Lakes are treated as ocean points with specified SSTs and sea ice concentration using the HadISST dataset in the atmosphere-only highresSST-present runs.
ECMWF-IFS	Great Lakes are modeled by 1D two-layer FLake model, which permits ice formation but lacks a lake circulation.
CNRM-CM6	Great Lakes are modeled by 1D two-layer FLake model, which permits ice formation but lacks a lake circulation.
MPI-ESM1-2	Great Lakes are modeled by a simple 1D one-layer (50-m thick) thermodynamic lake model, which permits ice formation but lacks a lake circulation.
GFDL CM4C192	Great Lakes are modeled by LM3's 1D lake model (one assigned depth for each lake), which permits ice formation but lacks a lake circulation.
FGOALS	Great Lakes are modeled by CLM4 1D 10-layer lake model (Zeng et al. 2002) using fixed 50-m bathymetry, which permits ice formation but lacks a lake circulation, in the atmosphere-only highresSST-present runs.
CMCC-CM2	Great Lakes are modeled by CLM4.5 1D 10-layer LISSS lake model (Subin et al. 2012) with spatially varying depths, which permits ice formation but lacks a lake circulation.

NICAM16-9S, with an estimated across-model average of 229 grid cells (Fig. S1). In FGOALS-f3-L, the Great Lakes are represented by only 12 grid cells spread across Lakes Superior, Huron, and Michigan, without including Lakes Ontario and Erie. Given insufficient documentation regarding lake treatment in HighResMIP (and broader CMIP) models and across-model inconsistencies in outputted variables as noted by Briley et al. (2021), these estimates of the number of Great Lakes grid cells are based on generating lake–land masks using output on lake fraction, percentage lake cover, land area fraction, bare soil fraction, upper and total soil moisture content, surface snow amount, and soil temperature. Most models include fairly reasonable spatial representations of the individual lakes' coastline morphology. Such detailed resolution can facilitate the simulation of broadscale lake-effect precipitation features.

Among the 12 families of HighResMIP GCMs examined here, the Great Lakes are treated by a spectrum of approaches (Table 2). A lake model is not applied in IPSL-CM6A-ATM, EC-Earth3P, INM-CM5-H, HadGEM3-GC31, MRI-AGCM, and NICAM16. The crudest lake treatment is present in IPSL-CM6A-ATM, as the atmospheric model is not coupled to an oceanic model in the high-resolution version and the Great Lakes are treated as bare soil using a coarse land–sea mask. The lakes' treatment sometimes differs between highresSST-present and hist-1950 simulations. For example, in EC-Earth3P, the Great Lakes are treated as water surfaces for grid cells with less than 50% land cover with LSTs and percent ice cover provided by the HadISST2 dataset in the prescribed-ocean highresSST-present runs, while in the fully coupled hist-1950 runs, Hudson Bay SSTs are extrapolated across the lakes. One-dimensional lake models are applied in six model families, including the two-layer FLake model in ECMWF-IFS and CNRM-CM6, a one-layer 50-m thick thermodynamic lake model in MPI-ESM1-2, the Land Model version 3 (LM3) lake model in GFDL CM4C192, the 10-layer lake model from the Community Land Model version 4 (CLM4) with fixed 50-m bathymetry in FGOALS, and the 10-layer Lake, Ice, Snow, and Sediment Simulator (LISSS) from CLM version 4.5 with spatially varying bathymetry in CMCC-CM2. Hereafter, the ensemble of GCMs that are coupled to 1D lake models is referred to as LakeMod, and the ensemble of GCMs without lake models is referred to as NoLakeMod (Table 2 caption).

b. *Observational datasets*

Daily gridded 1-km liquid-equivalent snowfall is retrieved from the National Weather Service's (NWS) National Operational Hydrologic Remote Sensing Center–Snow Data Assimilation

System (SNODAS) dataset (Barrett 2003; Clow et al. 2012), which integrates data from ground stations, satellite, airborne platforms, and a snow model (Carroll et al. 2001) and is used operationally by the National Oceanic and Atmospheric Administration's (NOAA) regional river forecast centers (Carroll et al. 2006). Gridded observational precipitation data are obtained from the National Aeronautics and Space Administration's (NASA) 1/8° North American Land Data Assimilation System version 2 (NLDAS-2) dataset (Xia et al. 2012), Oak Ridge National Laboratory's 1-km Daymet dataset (Thornton et al. 1997, 2014), and the NWS 1-km Analysis of Record for Calibration (AORC) dataset (Kitzmiller et al. 2018). Overlake eddy covariance-based measurements of SH and LH fluxes are obtained through the Great Lakes Evaporation Network (GLEN; Blanken et al. 2011; Spence et al. 2011, 2013; Lenters et al. 2013) at Granite Island (46.72°N, 87.40°W) and Stannard Rock (45.83°N, 85.15°W) on Lake Superior, Spectacle Reef (45.77°N, 84.15°W) on Lake Huron, White Shoal (45.83°N, 85.15°W) on Lake Michigan, and Long Point (42.57°N, 80.05°W) on Lake Erie. Of these sites, Stannard Rock is arguably the only one that can be classified as offshore, thereby limiting the representativeness of the GLEN measurements. The CoastWatch's Great Lakes Surface Environmental Analysis LST Dataset version 2 from NOAA's Great Lakes Environmental Research Laboratory (GLERL) provides lakewide daily mean LSTs, derived from Advanced Very High Resolution Radiometer composite imagery, which are highly consistent with buoy observations (Schwab et al. 1992, 1999). Lakewide-average percent ice cover is extracted from GLERL's Great Lakes Ice Atlas (Assel 2003, 2005; Wang et al. 2012). Through the ESGF, Great Lakes' LST and ice cover are also retrieved from the HadISST2 dataset, which supplies LST boundary conditions to some HighResMIP GCMs; the global HadISST2 dataset is evaluated here against the CoastWatch and Great Lakes Ice Atlas datasets given their known regional reliability in the GLB.

3. Results

a. Model assessment across the Great Lakes region

Annual mean climatological liquid-equivalent snowfall across the broader Great Lakes region (38°–52°N, 96°–72°W), encompassing the Midwest and Northeast United States, southern Ontario, and southern Quebec, is compared between prescribed-ocean highresSST-present simulations and coupled hist-1950 simulations from 23 HighResMIP GCMs and SNODAS data (Fig. 1). All of the models capture the observed high snowfall totals over Ontario and Quebec, while there are noteworthy across-model differences in the ability to capture lake-effect peaks and their associated magnitudes. The coarsest models, FGOALS-f3-L and CMCC-CM2-HR4 with local grid spacing of about 100 km, display minimal to no apparent signal of lake-effect snowfall (Fig. 1), despite their coupling to a lake model. Higher spatial resolution facilitates the capacity for GCMs with some Great Lake representation to simulate the region's distinct lake-effect zones and topographic influences but does not guarantee improved snowfall simulations over coarser versions and often leads to reduced climatological snowfall. By comparing lower- versus higher-spatial-resolution versions of the same GCM (e.g., FGOALS-f3, CMCC-CM2, and HadGEM3-GC31), it is apparent that snowfall patterns associated with topographic features, including the Great Lakes, Tughill Plateau, and Adirondack and Catskill Mountains, are more recognizable at higher resolution.

Spatial correlations are performed between HighResMIP-simulated and SNODAS annual climatological liquid-equivalent snowfall across the Great Lakes region, after interpolating model output to SNODAS' grid (Fig. 2a). The spatial correlations are high among all 34 combinations of models and scenarios/configurations (highresSST-present and hist-1950), ranging from 0.81 in the hist-1950 simulation of CNRM-CM5-1-HR to 0.97 in the hist-1950 simulation of CMCC-CM2-VHR4 (Fig. 2a). Across the 23 models, the spatial correlation is not significantly related to the models' grid spacing (Fig. 2b). There is little assurance that iteratively increasing the resolution from, say, 50 to 25 to 15 km (e.g., NICAM16) will improve the simulated spatial distribution of climatological snowfall (Fig. 2b). Higher spatial resolution leads to increased spatial correlations for CMCC-CM2, FGOALS-f3, and ECMWF-IFS, yet reduced correlations for NICAM16 (Fig. 2b). The across-model mean spatial correlation with observations is minimally impacted if results are partitioned as highresSST-present versus hist-1950 or as LakeMod versus NoLakeMod (Fig. 2b). This suggests that the spatial correlation between simulated and observed snowfall climatology is typically insensitive to the choice of a fully coupled model configuration versus prescribed-ocean climate model and to the choice of coupling to a 1D lake model. While expanding from an AMIP-style model to a fully coupled model or coupling the GCM to a lake model both result in more advanced representation of key interactive climate system processes and feedbacks, it simultaneously increases the opportunity for further biases to be introduced into the climate simulation rather than imposing observed LST/SST boundary conditions.

The mean bias of HighResMIP-simulated annual climatological liquid-equivalent snowfall is assessed compared to SNODAS for the Great Lakes region (Fig. 3a). The vast majority of HighResMIP models exhibit underestimated regional snowfall, especially CMCC-CM2 and FGOALS-f3, both applying CLM's lake model, with annual deficiencies of 30%–45% (Fig. 3a) (Gates and Rood 2021). Of the 34 model-scenario combinations, 91% are characterized by a negative bias in regionally averaged annual liquid-equivalent snowfall (Fig. 3a). There is no clear benefit of higher spatial resolution in terms of minimizing annual snowfall biases across the HighResMIP ensemble, demonstrating that higher-resolution models are not always superior to coarser models (Fig. 3b). When comparing simulations of the same model at different grid spacing, higher-resolution results in greater biases for NICAM16 and MPI-ESM1 and reduced biases for CMCC-CM2 and EC-Earth3P (Fig. 3b). Among the 11 models that were run for both configurations, the across-model mean bias is −18% for the fully coupled hist-1950 runs and −14% for the prescribed-ocean highresSST-present runs, with the bias

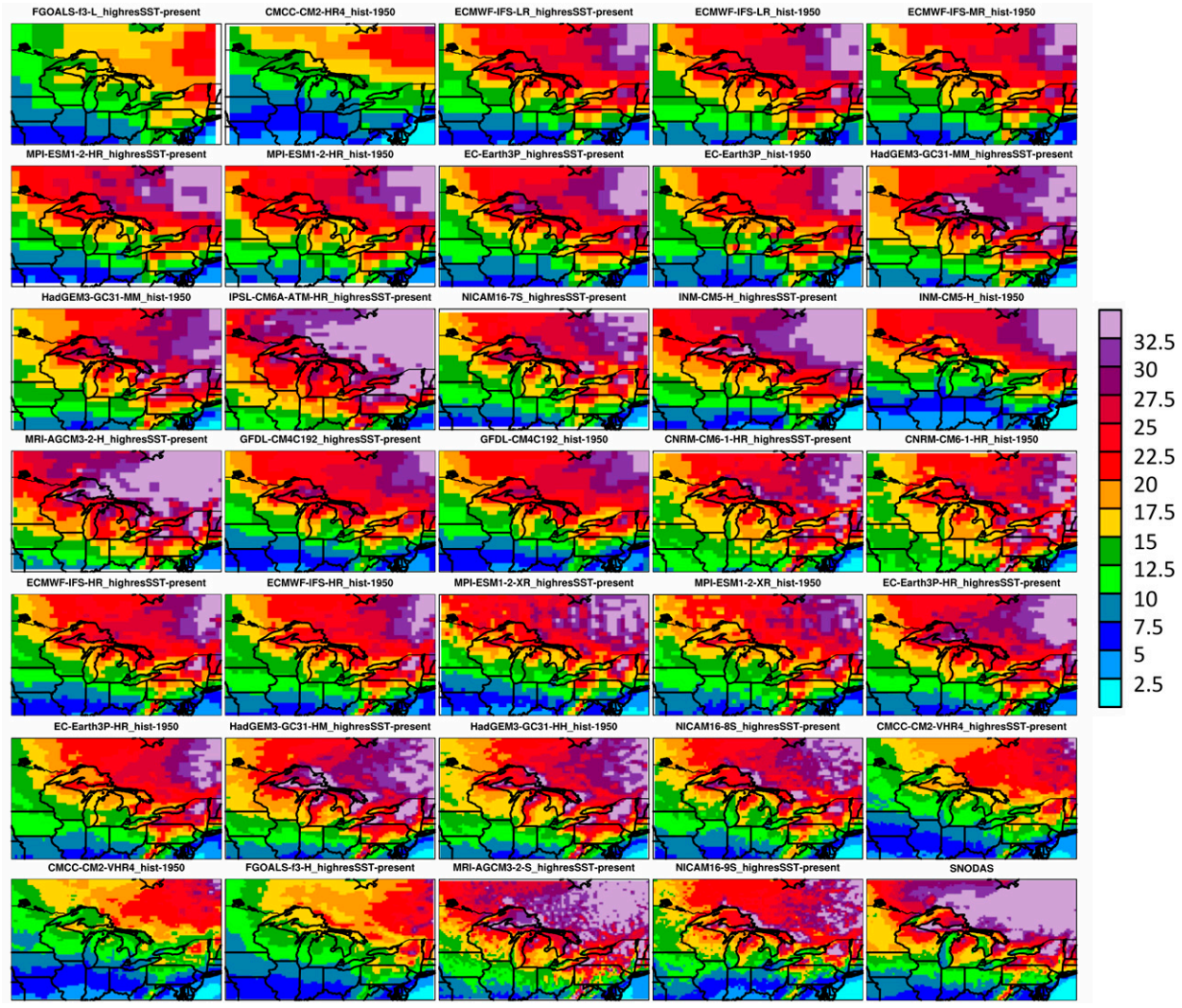

FIG. 1. Annual mean climatological liquid-equivalent snowfall (cm yr^{-1}) from (bottom right) SNODAS and HighResMIP models according to highresSST-present and hist-1950 simulations, in approximate order of increasing local resolution.

greater in the hist-1950 for 9 of 11 models (Fig. 3b). The fully coupled runs generally have greater snowfall deficiencies, especially for INM-CM5-H, with a coupled model run that prescribes 1950 lake conditions without dependence on HadISST2, and for EC-Earth3P, with a coupled model run that extrapolates Hudson Bay SSTs over the lakes (Figs. 3a,b). Negative biases in Great Lakes' LST and overlake turbulent fluxes lead to insufficient lake-effect snowfall in the fully coupled EC-Earth3P and EC-Earth3P-HR (discussed later). The average across-model bias in annual climatological liquid-equivalent snowfall in the Great Lakes region is significantly ($p < 0.01$) larger in LakeMod (−21.0%) than NoLakeMod (−7.6%) (Figs. 3a,b). Simulations with the greatest negative snowfall biases typically apply 1D lake models (Fig. 3b).

The root-mean-square difference (RMSD) is computed for each model and scenario between maps of simulated and SNODAS-based annual mean liquid-equivalent snowfall (Fig. 4a). Most models perform comparably well, except for notably poor performances (RMSD>7 cm yr^{-1}) by CMCC-CM2 and FGOALS-f3, both coupled to CLM's lake model, in the Great Lakes region (Fig. 4a). Higher spatial resolution leads to improved RMSDs for CMCC-CM2, FGOALS-f3, and EC-Earth3P but worse performance for MPI-ESM1 (Fig. 4b). Overall, higher resolution provides a GCM the opportunity to capture broadscale lake-effect snow patterns but does not guarantee improvement over coarser versions of the same model. Among 11 models with both highresSST-present and hist-1950 output, the across-model mean RMSD is 6.97 cm for fully coupled hist-1950 runs and 6.07 cm for prescribed-ocean highresSST-present runs, with a greater RMSD in hist-1950 runs for 10 of the 11 models, thereby indicating reduced skill in fully coupled models (Fig. 4b). The across-model mean RMSD is 31% higher ($p < 0.01$) for LakeMod compared to NoLakeMod, indicating that 1D lake model

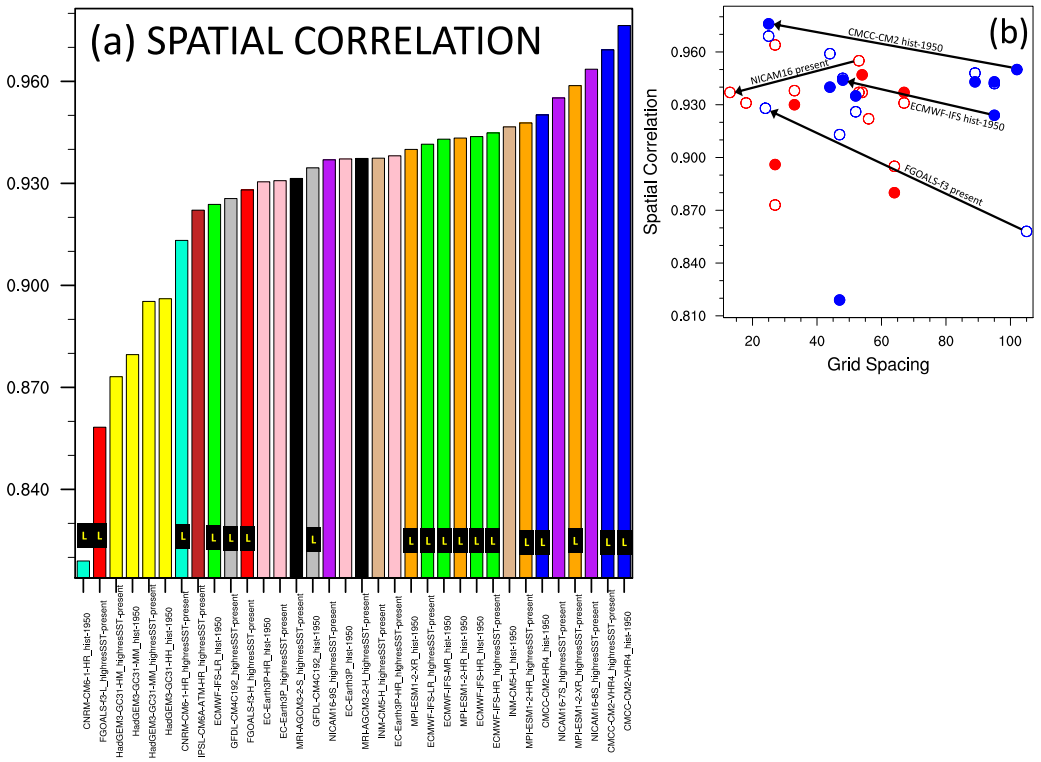

FIG. 2. (a) Spatial correlation between simulated and SNODAS annual mean climatological liquid-equivalent snowfall across the Great Lakes region (38°–52°N, 96°–72°W). LakeMod experiments, which include coupling to a 1D lake model, are identified with an "L." Experiments are plotted in order of increasing correlation. Models of the same family share the same colored bars. The mean spatial correlation is 0.931 for GCMs with a lake model and 0.926 for GCMs without a lake model, with no significant difference between these correlations. (b) Scatterplot of models' grid spacing (x axis, km) versus the spatial correlation (y axis) between simulated and SNODAS annual mean climatological liquid-equivalent snowfall across the Great Lakes region, as shown in (a). Blue (red) dots indicate the inclusion (exclusion) of a lake model. Filled (hollow) dots indicate coupled hist-1950 (uncoupled present-day) runs. Increased spatial resolution supports higher spatial correlations for CMCC-CM2, ECMWF-IFS, and FGOALS-IFS but lower correlations for NICAM16, as indicated by arrows. Among the eight models examined in this study at multiple spatial resolutions, the arrows indicate the four that exhibit the largest differences ($\geq \pm 0.02$) in spatial correlation between lower- and higher-resolution versions.

coupling usually reduces the regional snowfall performance (Fig. 4b).

The performance of four AMIP-style Diagnostic, Evaluation and Characterization of Klima (DECK) experiments, with 250-km grid spacing, is assessed for the Great Lakes region from CNRM-CM6-1, HadGEM3-GC31-LL, IPSL-CM6A-LR, and MPI-ESM1-2-LR, where LR indicates low resolution (not shown). This limited analysis explores the question if any benefits are realized by examining HighResMIP models relative to the standard-resolution CMIP6 models. Model evaluation focuses on the climatological patterns of annual liquid-equivalent snowfall across the Great Lakes region. Overall, the Great Lakes are hardly recognizable in the CMIP6 DECK experiments given their coarse spatial resolution. For MPI-ESM1-2, the number of lake grid cells in the region drops off rapidly from 131 in the XR (very high resolution) version, 30 in the HR (high resolution) version, and only 2 in the LR version, fewer than the actual number of Great Lakes. Somewhat surprisingly, the spatial correlation between SNODAS and simulated climatological annual liquid-equivalent snowfall is only modestly different between the coarse 250-km DECK runs and the HighResMIP runs. Both the coarse- and fine-resolution models can capture the basic regulation of climatological snowfall by latitude and elevation in the region, although the complex signature of lake-effect precipitation really requires the higher resolution. Compared to the DECK runs, HighResMIP simulations are generally characterized by reduced biases, especially in CNRM-CM6-1 (−19.7% in DECK versus −7.8% in HR) and HadGEM3-GC31 (−16.3% in DECK versus −2.8% in version MM and −2.1% in version HM). Furthermore, the HighResMIP runs are characterized by lower RMSD in CNRM-CM6-1 (25% less in HR compared to DECK) and HadGEM3-GC31 (15%–18% less in versions MM and HM compared to DECK), although the RMSD is only modestly different between the DECK and HighResMIP versions of IPSL-

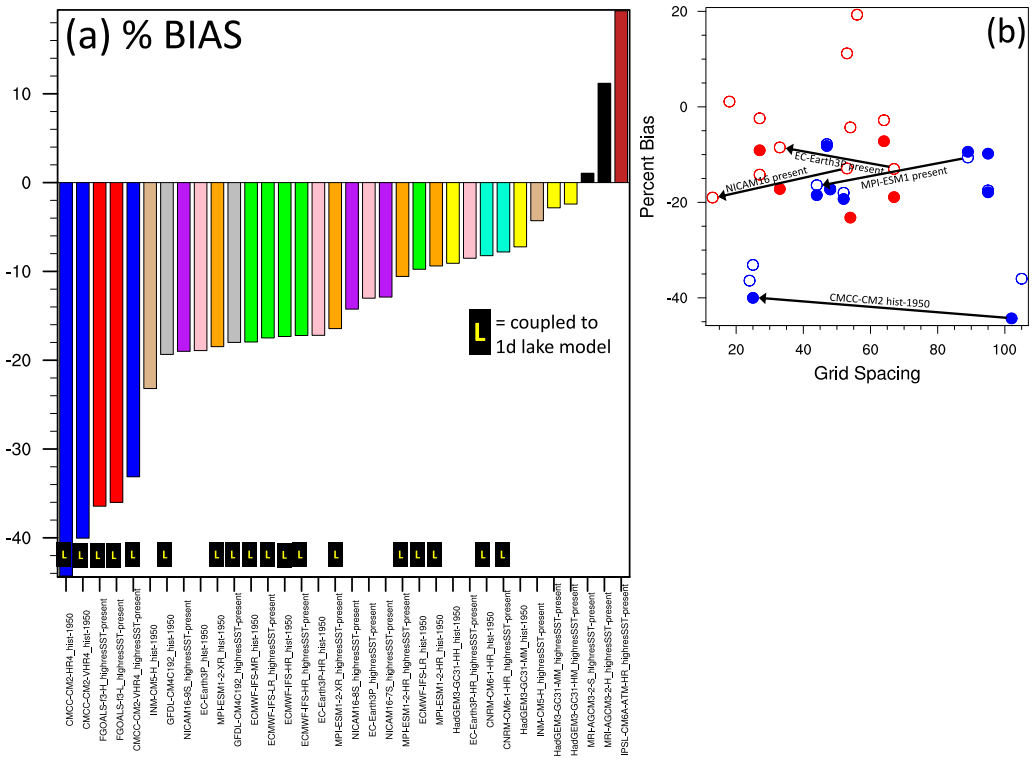

FIG. 3. (a) Percentage bias between simulated and SNODAS annual mean climatological liquid-equivalent snowfall across the Great Lakes region (38°–52°N, 96°–72°W). LakeMod experiments, which include coupling to a 1D lake model, are identified with an "L." Experiments are plotted in order from the most negative to most positive bias. Models of the same family share the same colored bars. The mean bias is −20.99% for GCMs with a lake model and −7.58% for GCMs without a lake model, with a significant difference ($p = 0.002$) between these correlations. (b) Scatterplot of models' grid spacing (x axis, km) versus the percentage bias (y axis) between simulated and SNODAS annual mean climatological liquid-equivalent snowfall across the Great Lakes region, as shown in (a). Blue (red) dots indicate the inclusion (exclusion) of a lake model. Filled (hollow) dots indicate coupled hist-1950 (uncoupled present-day) runs. Increased spatial resolution leads to greater biases for NICAM16 and MPI-ESM1 and lesser biases for EC-Earth3P and CMCC-CM2, as indicated by arrows. The arrows indicate two select models with increases in percentage bias at higher spatial resolution and two select models with decreases in percentage bias, with differences exceeding ±4%.

CM6A and MPI-ESM1-2. Examination of hourly to daily simulated snowfall easily reveals amorphous snowfall patterns in the DECK simulations that hardly resemble lake-effect snowstorms in contrast to the higher-resolution HighResMIP simulations, which capture some of the broad spatiotemporal features of such snowstorms. The DECK versions are clearly inappropriate to apply for lake-effect analysis.

b. *Focused assessment of lake-effect zones*

Analysis next zooms in geographically on the GLB (41°–50°N, 91°–75°W), where lake-effect snowfall is most active, with a focus on both the annual mean and seasonal cycle of liquid-equivalent snowfall (Fig. 5a, Fig. S2). Of the 34 combinations of HighResMIP models and scenarios/configurations (Fig. S2), 29 generate less annual snowfall than SNODAS' annual mean of 24.7 cm yr^{-1}, consistent with the earlier, broader regional discussion, with a notable negative bias downwind of Lake Superior. Increasing a HighResMIP model's spatial resolution seemingly results in inconsistent, unpredictable consequences, with reduced basinwide biases in annual liquid-equivalent snowfall for four models (e.g., −3.2 cm in 67-km EC-Earth3P versus −1.6 cm in 33-km EC-Earth3P-HR for highresSST-present) and amplified biases for four models (e.g., −2.8 cm in 53-km NICAM16-7S versus −3.6 cm in 13-km NICAM16-9S for highresSST-present) (Fig. S2). The LakeMod GCMs often simulate insufficient basinwide snowfall, characterized by a mean bias of −5.2 cm, while NoLakeMod GCMs typically perform better (significantly different, $p < 0.01$), with a mean bias of −1.5 cm (Fig. 5a, Fig. S2). GCMs that apply CLM's 1D lake model, namely, FGOALS and CMCC, substantially underproduce basinwide liquid-equivalent snowfall, averaging only 15.4 cm yr^{-1} (Fig. S2). Most (30 of 34) models and configurations produce an earlier peak in liquid-equivalent snowfall than SNODAS (observed peak in February) in the GLB, which is a bias that is especially notable with LakeMod GCMs (mean peak in December) (Fig. 5a, Fig. S2).

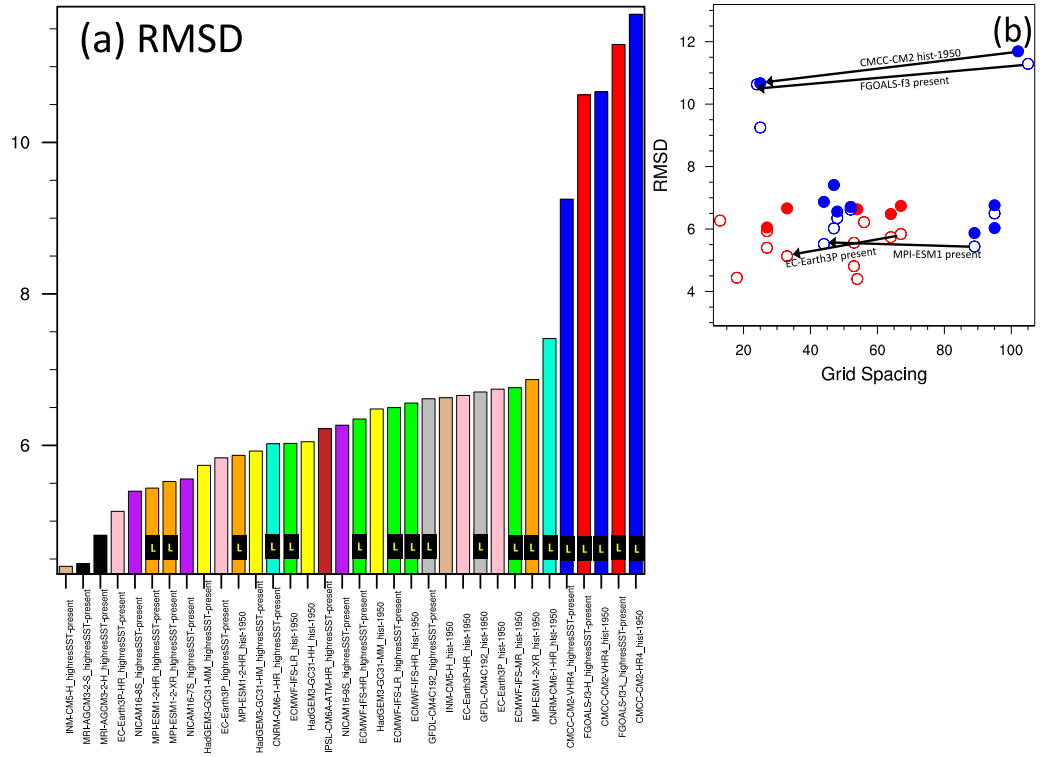

FIG. 4. (a) Root-mean-square difference (RMSD) between simulated and SNODAS annual mean climatological liquid-equivalent snowfall (cm yr^{-1}) across the Great Lakes region (38°–52°N, 96°–72°W). LakeMod experiments, which include coupling to a 1D lake model, are identified with an "L." Experiments are plotted in order of increasing RMSD. Models of the same family share the same colored bars. The mean RMSD is 7.57 cm yr^{-1} for GCMs with a lake model and 5.77 cm yr^{-1} for GCMs without a lake model, with a significant difference ($p = 0.003$) between these correlations. The RMSD is 31% greater in lake model-enabled GCMs than those GCMs without lake models. (b) Scatterplot of models' grid spacing (x axis, km) versus RMSD (cm yr^{-1}, y axis) between simulated and SNODAS annual mean climatological liquid-equivalent snowfall across the Great Lakes region, as shown in (a). Blue (red) dots indicate the inclusion (exclusion) of a lake model. Filled (hollow) dots indicate coupled hist-1950 (uncoupled present-day) runs. Increased spatial resolution leads to greater RMSD for MPI-ESM1 (only one of eight models, examined at different spatial resolutions, with a notable increase in RMSD) and lower RMSD for CMCC-CM2, FGOALS-f3, and EC-Earth3P (three models with the largest decrease in RMSD, of at least −0.66, at higher resolution), as indicated by arrows.

c. Contrasting lakes: Superior and Erie

The analysis further zooms in geographically by assessing the seasonal cycle of liquid-equivalent snowfall downwind of two contrasting lakes, namely, the vast, deep Lake Superior (Fig. 5b, Fig. S3) and smaller, relatively shallow Lake Erie (Fig. 5c, Fig. S4), with annual mean totals in SNODAS of 29.4 and 17.9 cm, respectively. Observed annual snowfall is greatest downwind of Lake Superior among the five lakes, as its massive water volume exhibits substantial thermal inertia and resulting large seasonal contrasts in water–air temperatures, along with extensive wind-induced fetch across its extensive surface area, in support of abundant lake-effect precipitation. Downwind of the northern lakes, most models undersimulate annual snowfall, including 91% of models and scenarios for Lake Superior (Fig. 5b, Fig. S3), 76% for Huron, and 71% for Ontario. Annual biases downwind of Lake Superior range from −53% in the hist-1950 simulation of CMCC-CM2-HR4 to +11% in the highresSST-present simulation of HadGEM3-GC31-HM (Fig. S3). For 9 of 11 models, the fully coupled hist-1950 runs produce less snowfall than the prescribed-ocean highresSST-present runs downwind of Lake Superior, with notable differences of −25.0% in INM-CM5-H and −20.7% in EC-Earth3P-HR (Fig. 5b, Fig. S3). In contrast, downwind of the southern lakes, Michigan and Erie (Fig. 5c, Fig. S4), a slight majority, 59%, of models and scenarios oversimulate annual snowfall. Downwind of Lake Erie, annual biases range from −39% in the hist-1950 simulation of CMCC-CM2-HR4 to +58% in the highresSST-present simulation of IPSL-CM6A-ATM-HR (Fig. S4). Most of the GCMs, especially those applying 1D lake models, produce insufficient annual snowfall, particularly downwind of Lake Superior related to excessive simulated ice cover (see section 3e). The across-model mean bias in annual liquid-equivalent snowfall downwind of Lake Superior is −8.3 cm for LakeMod GCMs versus −2.7 cm for NoLakeMod GCMs, with a significant ($p < 0.01$)

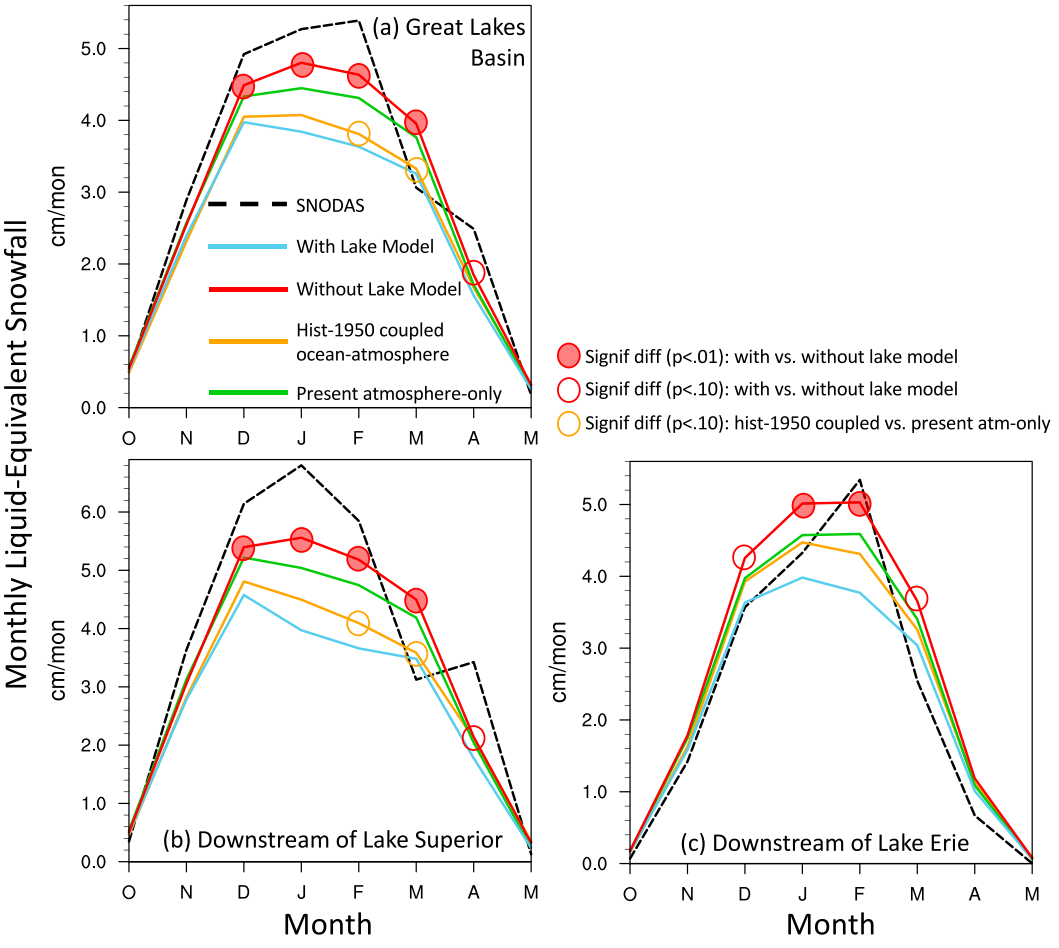

FIG. 5. Mean seasonal cycle of liquid-equivalent snowfall (cm month^{-1}) (a) across the Great Lakes basin (41°–50°N, 91°–75°W), (b) downwind of Lake Superior (46°–47°N, 90°–83°W), and (c) downwind of Lake Erie (41°–43°N, 82°–77°W). Results are shown from SNODAS with a black dashed line and HighResMIP across-model mean with colored solid lines, namely, runs including a lake model in blue, runs excluding a lake model in red, hist-1950 coupled ocean–atmosphere runs in orange, and present-day atmosphere-only runs in green. Filled red dots indicate significant ($p < 0.01$) differences between runs with lake models and runs without lake models, based on the Student's t test. Hollow red dots indicate significant ($p < 0.10$) differences between runs with lake models and runs without lake models. Hollow orange dots indicate significant ($p < 0.10$) differences between hist-1950 coupled ocean–atmosphere runs and present-day atmosphere-only runs.

difference (Fig. 5b). Downwind of Lake Superior, climatological monthly liquid-equivalent snowfall is significantly ($p < 0.01$) greater in the NoLakeMod ensemble than the LakeMod ensemble during December–March (Fig. 5b). The negative bias downwind of Lake Superior is pronounced for GCMs coupled to CLM's lake model, namely, FGOALS-f3 and CMCC-CM2, with an average bias of −13.4 cm (Fig. S3). Downwind of Lake Erie, the across-model mean bias in liquid-equivalent snowfall is −0.7 cm for LakeMod, significantly ($p < 0.01$) smaller than the +3.2-cm bias for NoLakeMod (Fig. 5c). Downwind of Lake Erie, climatological liquid-equivalent snowfall is significantly ($p < 0.01$) greater in the NoLakeMod ensemble than the LakeMod ensemble during January–February (Fig. 5c). Coupling to a 1D lake model often improves the integrated annual snowfall simulations (but not necessarily the seasonality) downwind of Lake Erie, unlike for deep Lake Superior. Across the lake-effect zone downwind of Lake Erie, 61% of models and scenarios display positive biases in annual liquid-equivalent snowfall (Fig. S4).

The seasonal timing of peak snowfall in SNODAS is January for Lakes Superior and Huron and February for Lakes Ontario, Michigan, and Erie (Figs. 5b,c, Figs. S3, S4). The majority of HighResMIP runs generate peak snowfall too early downwind of Lakes Superior (59% of models/scenarios peak in December, Fig. 5b, Fig. S3), Michigan (65% in January), Ontario (59% in January), and Erie (56% in January, Fig. 5c, Fig. S4).

d. Upwind versus downwind precipitation

A lake-effect ratio, representing the Great Lakes' seasonal influence on mean precipitation climatology, is computed

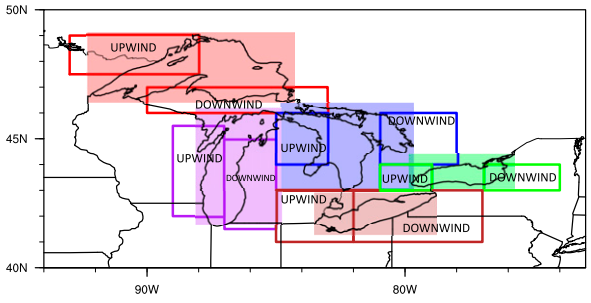

FIG. 6. Upwind and downwind lake-effect regions for Lakes Superior (red, upwind: 47.5°–49°N, 93°–88°W; downwind: 46°–47°N, 90°–83°W), Huron (blue, upwind: 44°–46°N, 85°–83°W; downwind: 44°–46°N, 81°–78°W), Ontario (green, upwind: 43°–44°N, 81°–79°W; downwind: 43°–44°N, 77°–74°W), Michigan (purple, upwind: 42°–45.5°N, 89°–87°W; downwind: 41.5°–45°N, 87°–85°W), and Erie (brown, upwind: 41°–43°N, 85°–82°W; downwind: 41°–43°N, 82°–77°W). The downwind lake-effect regions, with annual mean liquid-equivalent snowfall generally in excess of 15 cm in SNODAS, are largely consistent with those identified by Notaro et al. (2015a), Wiley and Mercer (2020, 2021), and an image obtained from the Department of Geography at Hunter College of the City University of New York. The upwind regions are determined based on the typical wind flow that generates lake-effect snow in the downwind regions (e.g. Notaro et al. 2015a; Pettersen et al. 2020).

based on dividing the climatological monthly mean overland precipitation in the region downwind of a Great Lake by the same variable upwind of the lake (Fig. 6). The seasonal cycle of the lake-effect ratio is presented for the GLB (averaged among the five lakes), only Lake Superior, and only Lake Erie in Fig. 7 and Figs. S5–S7 for 33 model–scenario combinations and three observational datasets, namely, NLDAS-2, Daymet, and AORC, in order to quantify observational uncertainty. The ratio is expected to differ among lakes depending on lake size, lake depth, and background climatological air temperature and wind. Averaged across observational datasets, the GLB lake-effect ratio ranges from 1.04 in June, with no evidence of the relatively cool lakes (compared to overlying air) dampening warm season precipitation, to 1.51 in January (Fig. 7a), when relatively mild LSTs support enhanced turbulent fluxes, ascending motion, instability, and downwind precipitation. The observational datasets are largely consistent when computed for the entire GLB (Fig. S5). The across-model mean ratio ranges from 1.10 in June to 1.39 in January, thereby capturing the seasonal evolution of the lake-effect ratio (Fig. 7a, Fig. S5). However, the lakes' amplifying effect on wintertime precipitation is underestimated by the multimodel mean (MMM) and erroneously simulated to be active even through summer (Fig. 7a). Based on the RMSD between the simulated and observed seasonal cycle of the GLB lake-effect ratio, the most successful models are MRI-AGCM3-2-S and EC-Earth3P-HR, both without lake models, and least successful models are CMCC-CM2-HR4 and MPI-ESM1-2-HR, both coupled to 1D lake models (Fig. S5). The largest errors in the lake-effect ratio are found during August (observed = 1.07) in the highresSST-present simulations of NICAM16-8S (MMM = 1.42) and FGOALS-f3-H (MMM = 1.39) (Fig. S5).

For Lake Superior, the observed lake-effect ratio exhibits an amplified seasonal cycle, ranging from 0.86 in June to 1.98 in January (Fig. 7b, Fig. S6), indicative of a modest dampening effect on summertime precipitation and pronounced enhancement of downwind wintertime precipitation. Observational uncertainty is substantial for Lake Superior, likely due to insufficient gauge coverage close to the lake (e.g., in Canada), as NLDAS-2 features a much larger lake-effect ratio than Daymet or AORC during December–February (Fig. S6). Overall, the models miss the observed dampening effect of Lake Superior on summertime precipitation and underestimate the lake's amplifying effect on wintertime precipitation, with a MMM lake-effect ratio that ranges from 1.02 in June to 1.57 in December (Fig. 7b, Fig. S6). Based on the RMSD between the simulated and observed seasonal cycle of Lake Superior's lake-effect ratio, the most successful models are HadGEM3-GC31-HM and HadGEM3-GC31-MM, both without lake models, and least successful models are FGOALS-f3-L and CMCC-CM2-HR4, both coupled to lake models (Fig. S6).

Compared to Lake Superior, the observed lake-effect ratio for Lake Erie exhibits weak seasonality, ranging from 1.04 in May to 1.29 in January, compared to 1.13 in April to 1.33 in January in the MMM (Fig. 7c, Fig. S7). Observational uncertainty is modest for Lake Erie, with Daymet inferring a greater wintertime lake-effect ratio than NLDAS-2 or AORC (Fig. S7). The MMM exaggerates the ratio during 10 of 12 calendar months, especially in August, but performs well during the cold season (Fig. 7c, Fig. S7). The most successful models that capture the seasonal cycle of Lake Erie's lake-effect ratio are ECMWF-IFS-HR and ECMWF-IFS-LR, both coupled to FLake, and least successful models are NICAM16-9S and NICAM16-8S, without lake models (Fig. S7). Overall, the Great Lakes' climatological influence on downwind precipitation is best captured using a 1D lake model for shallow lakes, like Erie, versus without a 1D lake model for deep lakes, like Superior.

Subsequent analysis of the GLB lake-effect ratio focuses on the November–March cold season (Fig. 8), when the lakes enhance downwind precipitation. All but 2 out of 33 models and scenarios underestimate the basinwide cold-season ratio, indicative of weaker-than-observed lake-effect precipitation processes (Fig. 8). The across-basin lake-effect ratio during November–March is most underestimated by CMCC-CM2-HR4 and ECMWF-IFS-LR/MR, both coupled to 1D lake models, and most reasonable for HadGEM3-GC31 and NICAM16, neither including lake models (Fig. 8). As evidence of the adverse impacts of 1D lake model coupling, the MMM bias in the cold season lake-effect ratio is −0.12 for LakeMod and −0.06 for NoLakeMod, with a statistically significant difference ($p < 0.01$) (Fig. 8 inset). Biases in the cold season lake-effect ratio are contrasted between Lakes Superior (Fig. 9) and Erie (Fig. 10). For Lake Superior, the cold season ratio is underestimated by 97% of the model–scenario combinations, suggesting weaker-than-observed lake effects on precipitation (Fig. 9). This ratio is vastly underestimated

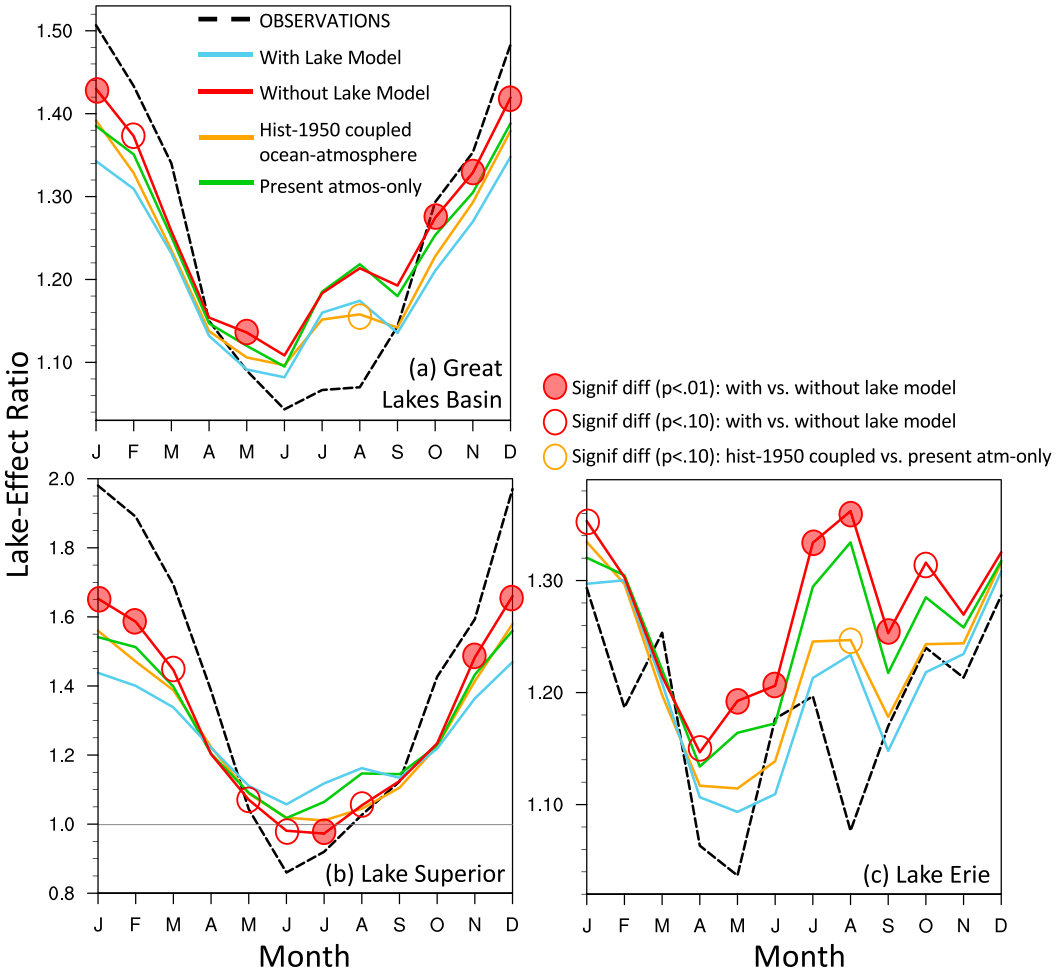

FIG. 7. Mean seasonal cycle of the ratio of monthly climatological precipitation between downwind and upwind lake-effect snow regions for the (a) entire Great Lakes basin or just Lakes (b) Superior and (c) Erie. For (a), one ratio (downwind/upwind) is computed for each Great Lake and then averaged among the five ratios. Results are shown from observations (averaged among NLDAS2, Daymet, and AORC) with a black dashed line and HighResMIP across-model mean with colored solid lines, namely, runs including a lake model in blue, runs excluding a lake model in red, hist-1950 coupled ocean–atmosphere runs in orange, and present-day atmosphere-only runs in green. Filled red dots indicate significant ($p < 0.01$) differences between runs with lake models and runs without lake models. Hollow red dots indicate significant ($p < 0.10$) differences between runs with lake models and runs without lake models. Hollow orange dots indicate significant ($p < 0.10$) differences between hist-1950 coupled ocean–atmosphere runs and present-day atmosphere-only runs.

by CMCC-CM2-HR4 and FGOALS-f3-L/H, both including lake models, but reasonable in NICAM16 and HadGEM3-GC3, both without lake models (Fig. 9). The across-model mean bias in cold season lake-effect ratio for Lake Superior is −0.42 for LakeMod and −0.26 for NoLakeMod, with a significant difference ($p < 0.01$) between ensembles (Fig. 9 inset). While nearly all models struggle to fully capture the strong enhancement of cold season precipitation by Lake Superior, those models that are coupled to 1D lake models exhibit greater deficiencies (Fig. 9). In contrast, 66% of the 33 model-scenario combinations overestimate the cold season lake-effect ratio for Lake Erie, suggesting stronger-than-observed lake-effect precipitation processes in most HighResMIP GCMs (Fig. 10). The cold season lake-effect ratio is most underestimated by NICAM16-7S and CNRM-CM6-1-HR and most reasonable in NICAM16-9S and ECMWF-IFS-HR (Fig. 10). Lake Erie's lake-effect ratio is largely insensitive to lake model coupling, as the mean bias in the cold season ratio is +0.02 for LakeMod versus +0.05 for NoLakeMod (insignificant difference) (Fig. 10 inset).

e. LST climatology

To better understand the HighResMIP GCMs' performance in representing lake–atmosphere interactions and resulting lake-effect precipitation in the GLB, the analysis

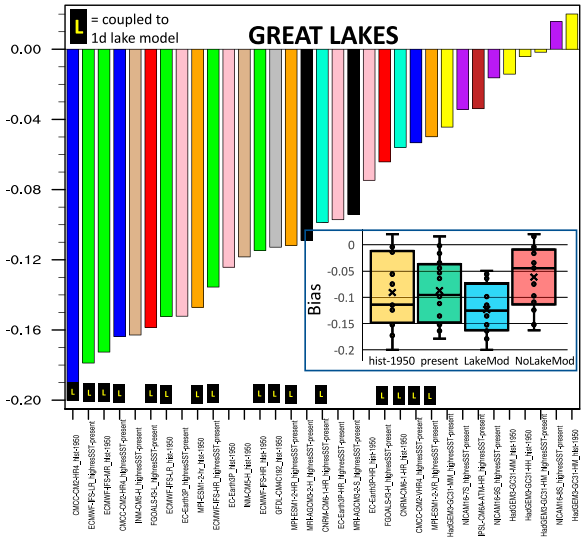

FIG. 8. Bias in the mean ratio (downwind/upwind) of November–March climatological precipitation between downwind and upwind lake-effect snow regions among 33 model–scenario combinations. One ratio is computed for each Great Lake and then averaged among the five ratios. The bias is assessed against the observed ratio, computed as an average among NLDAS-2, Daymet, and AORC. LakeMod HighResMIP models, which are coupled to a 1D lake model, are identified with the letter "L." The smaller inset figure is a box-and-whiskers plot of the mean bias across models for the hist-1950, present, LakeMod, and NoLakeNod runs.

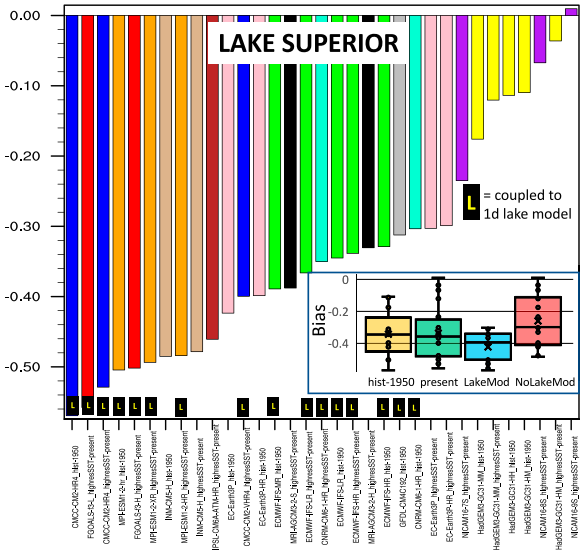

FIG. 9. Bias in the mean ratio (downwind/upwind) of November–March climatological precipitation between the downwind and upwind lake-effect snow region of Lake Superior among 33 model–scenario combinations. The bias is assessed against the observed ratio, computed as an average among NLDAS-2, Daymet, and AORC. LakeMod HighResMIP models, which are coupled to a 1D lake model, are identified with the letter "L." The smaller inset figure is a box-and-whiskers plot of the mean bias across models for the hist-1950, present, LakeMod, and NoLakeNod runs.

here focuses on the simulated mean seasonal cycle of LST compared to CoastWatch observations (Fig. 11). LakeMod GCMs typically generate negative wintertime and positive summertime LST biases and anomalously early stratification (approximately when LSTs reach 4°C). Simulated wintertime LSTs are too low among most GCMs, with the bias more pronounced among LakeMod GCMs (Fig. 11). Conversely, the absence of a lake model and application of HadISST2 water temperatures as LST boundary conditions does not ensure reasonable Great Lakes' LSTs. For example, the fully coupled EC-Earth3P extrapolates Hudson Bay SSTs from HadISST2 across the western Great Lakes and North Atlantic SSTs from HadISST2 across the eastern Great Lakes (rather than using Great Lake SST values from HadISST2), resulting in negative LST biases over Superior, Huron, and Michigan and positive biases over Ontario and Erie.

Simulated annual LST biases and RMSDs, compared to CoastWatch data, are greatest for Lake Superior and least for Lake Erie (Figs. 11a,e). Averaged among the five lakes, the mean annual LST bias is −1.6°C in LakeMod versus −1.1°C in NoLakeMod, with RMSDs of 4.9° and 2.6°C, respectively. January–February LSTs are significantly ($p < 0.01$) lower in LakeMod than NoLakeMod, with vast cold biases in LakeMod, ranging from −13.0°C for Superior to −6.2°C for Erie, compared to more modest biases in NoLakeMod, from −4.8°C for Superior to −0.7°C for Erie (Figs. 11a,e). The greatest winter LST cold bias is found in CMCC-CM2-HR4, coupled to CLM's lake model.

Imposing HadISST2 water temperatures as Great Lakes' boundary conditions, rather than coupling to a 1D lake model, typically results in more reasonable year-round LSTs, although the coarse global HadISST2 dataset may not be a highly reliable source of Great Lakes' LSTs as evident by inconsistencies with CoastWatch observations. Based on comparing Great Lakes' climatological LSTs between HadISST2 and CoastWatch since 1995, November–March LSTs are too warm in HadISST2 for Lake Erie by +0.6°C and too cold in HadISST2 for Lakes Michigan and Ontario by −0.4°C (not shown); the largest difference is noted for Lake Erie in February, with HadISST2 LSTs exceeding CoastWatch LSTs by +1.7°C.

Application of HadISST2 ice cover as Great Lakes' boundary conditions in the NoLakeMod GCMs induces critical impacts on overlake turbulent fluxes and resulting lake-effect precipitation. Compared to the Great Lakes Ice Atlas for December–April since 1995, HadISST2-estimated percent ice cover is negatively biased over Lake Erie by −16.5% (peaking at −37.8% during February) and positively biased over Lake Superior by +5.0% (peaking at +13.6% during February). These HadISST2-related lake ice cover biases support excessive turbulent fluxes over Lake Erie (favoring greater lake-effect snowfall in INM-CM5-H, HadGEM3-GC31, MRI-AGCM, NICAM16, and EC-Earth3P) and insufficient fluxes over Lake Superior.

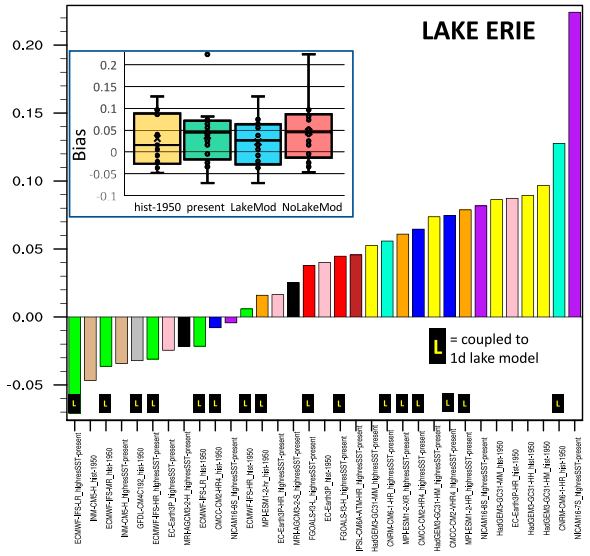

FIG. 10. Bias in the mean ratio (downwind/upwind) of November–March climatological precipitation between the downwind and upwind lake-effect snow region of Lake Erie among 33 model–scenario combinations. The bias is assessed against the observed ratio, computed as an average among NLDAS-2, Daymet, and AORC. LakeMod HighResMIP models, which are coupled to a 1D lake model, are identified with the letter "L." The smaller inset figure is a box-and-whiskers plot of the mean bias across models for the hist-1950, present, LakeMod, and NoLakeNod runs.

f. Overlake SH fluxes

Lake-effect snow is largely driven by turbulent heat and moisture fluxes between the lakes and atmosphere, namely, sensible and latent heat fluxes, and their impacts on atmospheric stability, moisture, and temperature. Therefore, making an accurate representation of these lake–atmosphere fluxes is necessary to capture lake-effect precipitation processes. Compared to GLEN observations, the HighResMIP GCMs generally underestimate SH fluxes over the deeper lakes and overestimate them over relatively shallow Lake Erie (Fig. 12). Annual SH flux biases are smaller for Lake Superior among NoLakeMod GCMs (Fig. 12a) and smaller for Lake Erie among LakeMod GCMs (Fig. 12d). The RMSD in annual SH flux over Lake Superior between HighResMIP GCMs and GLEN observations is higher in LakeMod (36.5 W m^{-2}) than NoLakeMod (25.6 W m^{-2}). In contrast, the RMSD in annual SH flux over Lake Erie is lower in LakeMod GCMs (14.1 W m^{-2}) than NoLakeMod (28.4 W m^{-2}). The seasonal cycle of overlake SH fluxes is best represented by HadGEM3-GC31-MM (without a lake model) for Lakes Superior and Huron, MPI-ESM1-2-HR (coupled to a lake model) for Lake Michigan, and ECMWF-IFS-HR (coupled to a lake model) for Lake Erie.

At the GLEN sites, mean SH fluxes peak in November over the southern lakes, Michigan and Erie (Figs. 12c,d), and January over the northern lakes, Superior and Huron (Figs. 12a,b). Due to the aforementioned LST biases, simulated peak SH fluxes are typically too early for the colder northern lakes and too late for the warmer southern lakes, compared to GLEN measurements. Coupling to a 1D lake model often encourages overlake SH fluxes to peak too early over Lakes Superior and Huron (Figs. 12a,b). Based on comparing the seasonality of overlake SH fluxes for Lake Superior in the HighResMIP models with GLEN measurements, the most notable discrepancies are found in FGOALS-f3-H/L coupled to CLM's lake model, with a simulated May peak, and IPSL-CM6A-ATM-HR (treats the lakes as bare soil), with a simulated July peak.

During the midwinter months of January–February, simulated overlake SH fluxes in LakeMod are significantly ($p < 0.01$) weaker than in NoLakeMod for Lakes Superior, Huron, and Erie (Figs. 12a,b,d). Lake model coupling leads to an amplified negative bias in SH flux during January–February for Lakes Superior (−77.2 W m^{-2} in LakeMod versus −5.0 W m^{-2} in NoLakeMod, Fig. 12a) and Huron (−74.2 W m^{-2} versus −35.6 W m^{-2}, Fig. 12b), a dampened positive bias for Lake Michigan (+4.5 W m^{-2} in LakeMod versus +45.7 W m^{-2} in NoLakeMod, Fig. 12c), and elimination of a positive bias for Lake Erie (−2.4 W m^{-2} versus +36.4 W m^{-2}, Fig. 12d). The fully coupled hist-1950 runs typically produce less SH fluxes over Lake Superior during January–February than the prescribed-ocean highresSST-present runs (Fig. 12a), as seen in 7 of 8 GCMs containing output from both scenarios, especially EC-Earth3P-HR (−91.3 W m^{-2} bias in hist-1950 versus −20.8 W m^{-2} in highresSST-present) and EC-Earth3P, which are characterized by excessively cold lake temperatures. Regarding Lake Erie, the fully coupled models often produce more overlake sensible heat fluxes during February–March than their prescribed-ocean versions (Fig. 12d), especially for EC-Earth3P and EC-Earth3P-HR which are characterized by large LST warm biases in the fully coupled models; specifically, the February–March mean bias in overlake SH flux on Lake Erie in EC-Earth3P is +18.1 W m^{-2} in the highresSST-present runs versus +105.0 W m^{-1} in the hist-1950 runs.

g. Overlake LH fluxes

Compared to GLEN observations, the HighResMIP GCMs generally underestimate LH fluxes over the northern lakes, Superior and Huron (Figs. 13a,b), and overestimate them over the southern lakes, Michigan and Erie (Figs. 13c,d), with the greatest annual LH flux biases, +32.0 W m^{-2} in NoLakeMod and +28.4 W m^{-2} in LakeMod, found over Lake Erie. The RMSD in annual LH flux, comparing HighResMIP models and GLEN measurements, is lower for NoLakeMod than LakeMod, including 22.1 W m^{-2} in NoLakeMod versus 49.2 W m^{-2} in LakeMod for Lake Superior. The seasonal cycle of overlake LH fluxes is best represented by HadGEM3-GC31-HH for Lakes Superior and Huron, EC-Earth3P-HR for Lake Michigan, and NICAM16-9S for Lake Erie, all without lake models.

At the GLEN sites, mean LH fluxes peak earlier over the southern lakes, namely, Erie in September (Fig. 13d) and Michigan in October (Fig. 13c), and later over the northern

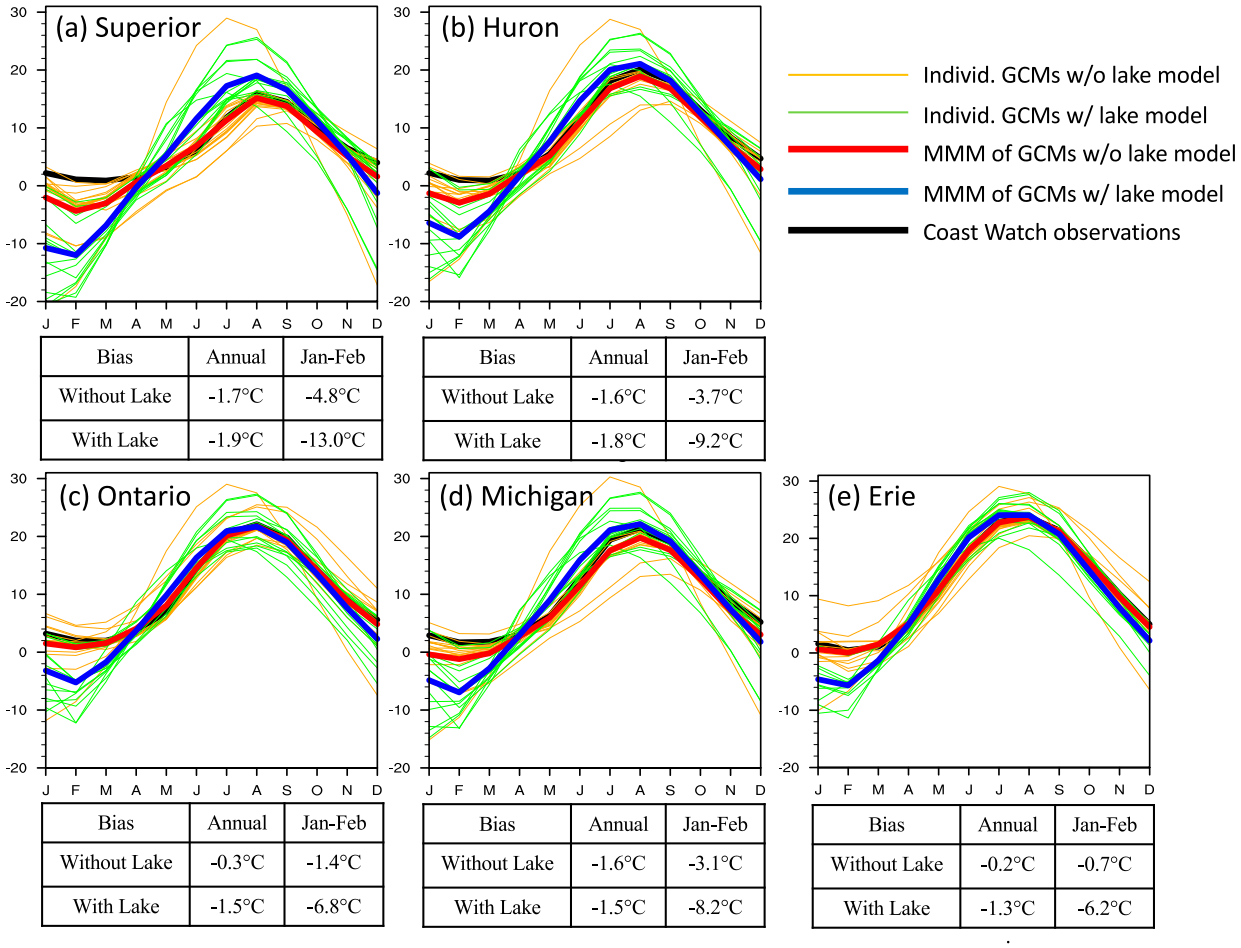

Bias	Annual	Jan-Feb
Without Lake	-1.7°C	-4.8°C
With Lake	-1.9°C	-13.0°C

Bias	Annual	Jan-Feb
Without Lake	-1.6°C	-3.7°C
With Lake	-1.8°C	-9.2°C

Bias	Annual	Jan-Feb
Without Lake	-0.3°C	-1.4°C
With Lake	-1.5°C	-6.8°C

Bias	Annual	Jan-Feb
Without Lake	-1.6°C	-3.1°C
With Lake	-1.5°C	-8.2°C

Bias	Annual	Jan-Feb
Without Lake	-0.2°C	-0.7°C
With Lake	-1.3°C	-6.2°C

FIG. 11. Mean seasonal cycle of LSTs (°C) for each of the Great Lakes from CoastWatch observations (black) and HighResMIP models. For the model results, red indicates the multimodel mean (MMM) for NoLakeMod GCMs, blue indicates the MMM for LakeMod GCMs, yellow indicates each individual NoLakeMod GCM, and green indicates each individual LakeMod GCM. The annual mean and January–February mean biases in LST for the ensemble set with lake model coupling and without lake model coupling are listed below each panel.

lakes, namely, Superior and Huron in January (Figs. 13a,b). Peak evaporation typically occurs 2–3 months too early when using a lake model, especially across the northern lakes (Figs. 13a,b). Five HighResMIP GCMs simulate an erroneous LH flux peak during summer over Lake Superior, including four LakeMod GCMs (MPI-ESM1-2-HR, CMCC-CM3-VHR4, FGOALS-F3-H, and FGOALS-F3-L) and one NoLakeMod GCM, IPSL-CM6A-ATM-HR, which treats the Great Lakes as land; the use of HadISST2 as LST boundary conditions in many GCMs avoids this erroneous seasonal timing. Simulated LH fluxes during January–February are significantly ($p < 0.01$) lower across Lakes Superior, Huron, Michigan, and Erie in LakeMod than NoLakeMod (Fig. 13), including biases over Lake Superior of -71.9 W m^{-2} in LakeMod versus -28.6 W m^{-2} in NoLakeMod. Typically, 1D lake models vastly underestimate wintertime SH and LH fluxes over Lake Superior (Figs. 12a, 13a). Averaged among INM-CM5-H, HadGEM3-GC31, MRI-AGCM, NICAM16, and EC-Earth3P, all of which apply HadISST2 LST boundary conditions, the mean LH flux bias during February over Lake Erie is $+28.0$ W m^{-2}, with the substantial positive bias likely associated with insufficient Lake Erie ice cover in HadISST2. The fully coupled hist-1950 simulations typically produce less LH fluxes over Lake Superior during January–February than the prescribed-ocean highresSST-present simulations (Fig. 13a), as seen in 6 of 8 GCMs containing output from both scenarios, especially for EC-Earth3P-HR and EC-Earth3P. Regarding Lake Erie, the prescribed-ocean models often generate more reasonable wintertime overlake LH fluxes than the fully coupled models (Fig. 13d).

To assess the implications of overlake LH biases on downwind snowfall biases, scatterplots are generated for Lakes Superior (Fig. S8a) and Erie (Fig. S8b) of simulated LH flux biases (compared to GLEN) versus simulated mean liquid-equivalent snowfall biases (compared to SNODAS) during December–March. The across-model correlation between these two biases is higher for Lake Superior (Fig. S8a), at 0.77 ($p < 0.01$), than for Lake Erie (Fig. S8b), at 0.33 ($p = 0.06$).

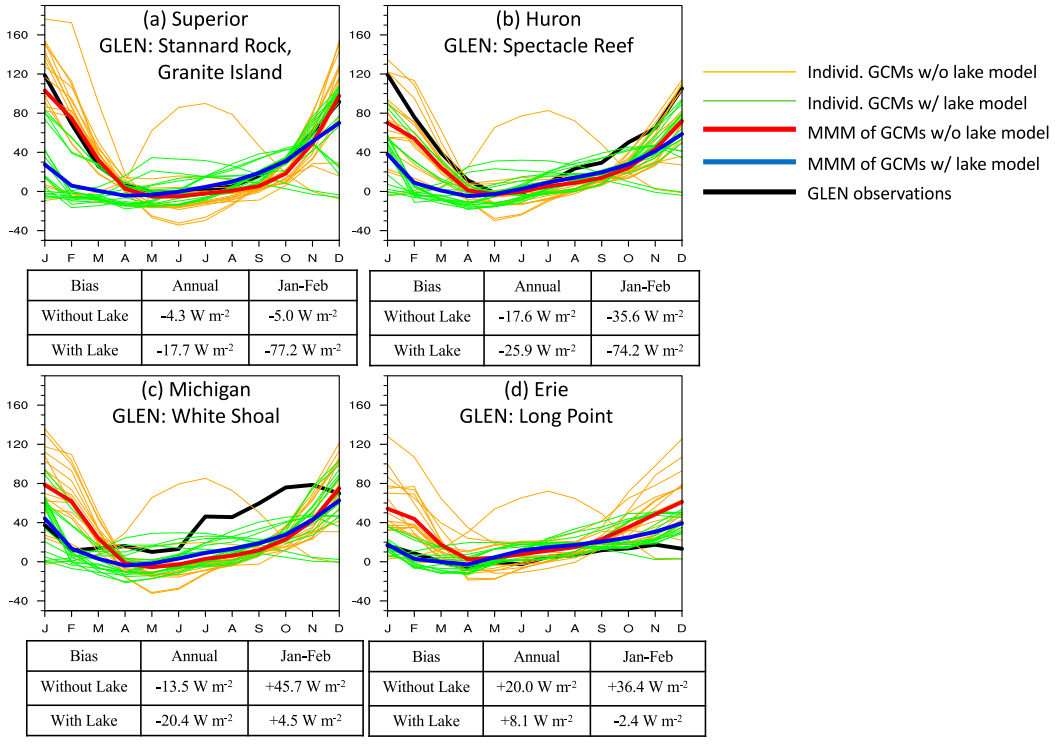

FIG. 12. Mean seasonal cycle of overlake sensible heat flux (W m^{-2}) for Lakes (a) Superior, (b) Huron, (c) Michigan, and (d) Erie from the Great Lakes Evaporation Network (GLEN) overlake measurements (black) and HighResMIP models. Model results are presented as lake-average. GLEN results are based on data for Stannard Rock and Granite Island (average of two sites) for Lake Superior, for Spectacle Reef for Lake Huron, for White Shoal for Lake Michigan, and for Long Point for Lake Erie. For the model results, red indicates the MMM for NoLakeMod GCMs, blue indicates the MMM for LakeMod GCMs, yellow indicates each individual NoLakeMod GCM, and green indicates each individual LakeMod GCM. The annual mean and January–February mean biases in overlake sensible heat flux for the ensemble set with lake model coupling and without lake model coupling are listed below each panel.

These correlations imply that deficient evaporation over Lake Superior corresponds to insufficient downwind lake-effect snowfall in HighResMIP GCMs (especially LakeMod), yet Lake Erie evaporation biases among HighResMIP GCMs only modestly translate into downwind snowfall biases. Regarding Lake Superior, the models largely underestimate overlake LH fluxes and downwind snowfall in December–February. The effect of deficient lake-effect snowfall due to insufficient Lake Superior evaporation is most distinct during January–February, based on replotting Fig. S8a by month (not shown).

4. Discussion and conclusions

The current study evaluates the capacity of high-resolution GCMs in the HighResMIP multimodel ensemble to accurately represent lake–atmosphere interactions and resulting lake-effect snowfall within the GLB. Analysis focuses on 74 simulations of either prescribed-ocean highresSST-present or fully coupled hist-1950 configurations from 23 GCMs, each with a spatial grid spacing of approximately 100 km or finer. The individual HighResMIP models treat the Great Lakes with a spectrum of approaches, including as land or ocean grid cells in NoLakeMod GCMs or with a 1D lake model in LakeMod GCMs, none of which are adequate for representing the complex nature of seasonal lake temperature and ice cover evolution and its impact on lake–atmosphere interactions. The main findings are outlined below.

1) The coarsest HighResMIP models examined here, with a grid spacing close to 100 km, display minimal to no apparent signal of lake-enhanced snowfall (Fig. 1). The same deficiency exists in most CMIP Diagnostic, Evaluation and Characterization of Klima (DECK) experiments due to their coarser resolution than in HighResMIP. Notaro et al. (2015a) previously noted that most GCMs are insufficient modeling tools for capturing lake-effect snowstorms due to coarse spatial resolution, inadequate representation of regional topography, struggles with modeling mesoscale circulations and convection, and underrepresentation of the Great Lakes (Briley et al. 2021; Minallah and Steiner 2021). Prior studies (Hjelmfelt and Braham 1983; Warner and Seaman 1990; Sousounis and Fritsch 1994; Ballentine et al. 1998; Notaro et al. 2013a) have

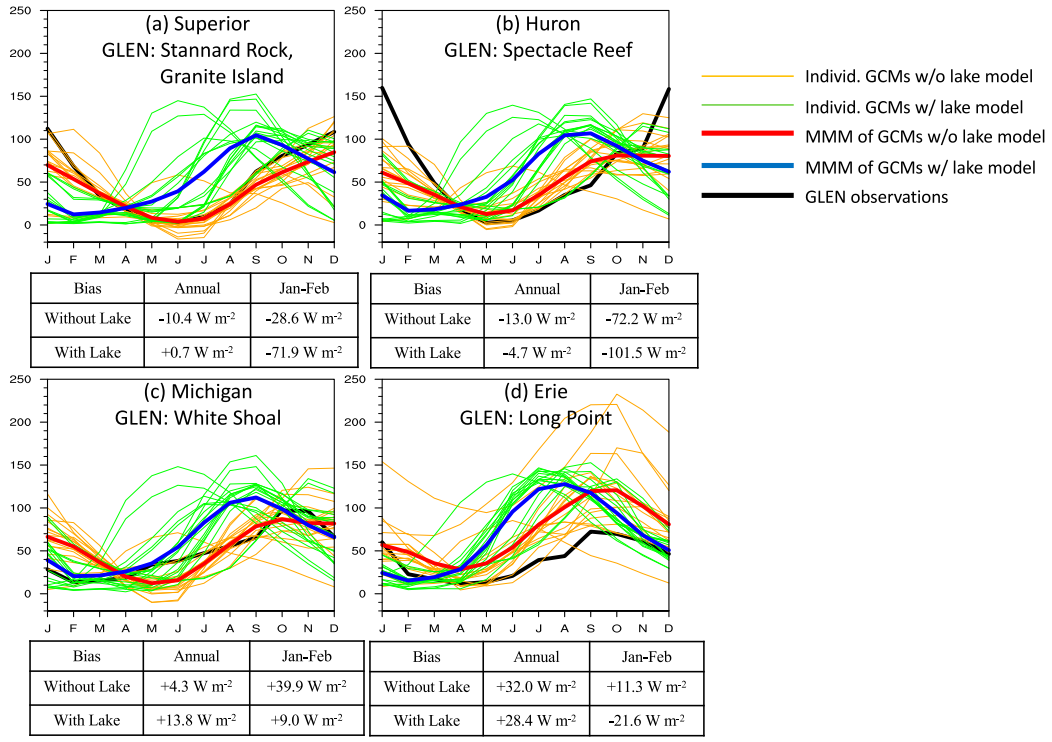

Bias	Annual	Jan-Feb
Without Lake	-10.4 W m^{-2}	-28.6 W m^{-2}
With Lake	+0.7 W m^{-2}	-71.9 W m^{-2}

Bias	Annual	Jan-Feb
Without Lake	-13.0 W m^{-2}	-72.2 W m^{-2}
With Lake	-4.7 W m^{-2}	-101.5 W m^{-2}

Bias	Annual	Jan-Feb
Without Lake	+4.3 W m^{-2}	+39.9 W m^{-2}
With Lake	+13.8 W m^{-2}	+9.0 W m^{-2}

Bias	Annual	Jan-Feb
Without Lake	+32.0 W m^{-2}	+11.3 W m^{-2}
With Lake	+28.4 W m^{-2}	-21.6 W m^{-2}

FIG. 13. Mean seasonal cycle of overlake latent heat flux (W m^{-2}) for Lakes (a) Superior, (b) Huron, (c) Michigan, and (d) Erie from the Great Lakes Evaporation Network (GLEN) overlake measurements (black) and HighResMIP models. Model results are presented as lake-average. GLEN results are based on data for Stannard Rock and Granite Island (average of two sites) for Lake Superior, for Spectacle Reef for Lake Huron, for White Shoal for Lake Michigan, and for Long Point for Lake Erie. For the model results, red indicates the MMM for NoLakeMod GCMs, blue indicates the MMM for LakeMod GCMs, yellow indicates each individual NoLakeMod GCM, and green indicates each individual LakeMod GCM. The annual mean and January–February mean biases in overlake latent heat flux for the ensemble set with lake model coupling and without lake model coupling are listed below each panel.

generally concluded that a horizontal grid spacing of 20–30 km or finer is needed to model lake-effect snowfall at the meso-β scale and GCMs with a grid spacing on the order of hundreds of kilometers are unable to resolve this phenomenon (Kunkel et al. 2002). Among the HighResMIP models, higher resolution does not assure improved snowfall simulations across the Great Lakes region over coarser model versions and often amplifies snowfall biases (Figs. 2–4). While HighResMIP's goal is to evaluate the potential benefits of increasing horizontal resolution without additional GCM modifications, such an approach is insufficient for advancing the representation of lake-effect precipitation in the GLB when the lakes' representation as land grid cells, ocean grid cells, or 1D lake columns is clearly oversimplified. This broad conclusion was likewise reached by Bador et al. (2020), in an assessment of global overland precipitation extremes produced by the HighResMIP GCMs in PRIMAVERA, the European Union Horizon 2020 project, who determined that higher resolution alone is insufficient to systematically improve simulated precipitation extremes as improvements to the dynamical core and physical parameterizations are likely needed.

2) Most HighResMIP GCMs, particularly those coupled to 1D lake models, underestimate annual liquid-equivalent snowfall in the Great Lakes region (Fig. 5a, Fig. S2), especially downwind of Lake Superior (Fig. 5b, Fig. S2), with more pronounced snowfall deficiencies often generated by fully coupled hist-1950 simulations (Fig. 5a). In contrast, both Minallah and Steiner (2021) and Almazroui et al. (2021) determined that the CMIP6 DECK ensemble produces excessive winter–spring precipitation in this region. Snowfall downstream of Lake Superior is more accurately simulated by NoLakeMod GCMs (Fig. 5b), while LakeMod GCMs perform better downstream of Lake Erie (Fig. 5c). Notaro et al. (2013a) likewise noted that RegCM4 coupled to a 1D lake model generates more realistic snowfall totals downwind of Lake Erie than Lake Superior due to Erie's less extreme biases in LST and ice cover. Observational snow datasets exhibit notable inconsistencies in the study region due to spatial gaps in the lake-effect zones (Notaro et al. 2021), leading to some uncertainty in the HighResMIP evaluation. Expanded observational data collection is needed across the GLB, both over lakes (precipitation, SH, LH) and land (snowfall).

3) The observed lake-effect ratio indicates that Lake Superior (Fig. 7b, Fig. S6), due to its large thermal inertia and resulting impacts on lake–atmosphere temperature contrasts and atmospheric stability, supports a pronounced enhancement of wintertime precipitation and reduction in summertime precipitation, consistent with Holman et al. (2012). The HighResMIP ensemble underestimates this wintertime enhancement across the GLB and lacks the summertime reduction in downwind precipitation, indicative of underrepresented lake–atmosphere interactions (Figs. 7a, 8, Fig. S5). The lakes' climatological influence on downwind precipitation is best captured using a 1D lake model for shallow Lake Erie (Figs. 7c, 10, Fig. S7) versus without a 1D lake model for deep Lake Superior (Figs. 7b, 9, Fig. S6), as 1D lake models were never designed to simulate deep, dynamic lakes. LakeMod typically exaggerates the amplitude of LST's seasonal cycle and therefore underestimates the amplitude of lake–atmosphere temperature contrasts (Fig. 11), thereby weakening lake feedbacks on downwind precipitation (Fig. 8). Excessive ice cover generated by 1D lake models dampens lake evaporation's contribution to lake-effect precipitation, thereby shortening the lake-effect unstable season (Notaro et al. 2013a). These LST and ice cover biases, associated with 1D lake models, can be expected for other large mid- to high-latitude lakes worldwide.
4) LakeMod GCMs typically generate negative wintertime and positive summertime LST biases (Fig. 11), which dampen lake–air temperature contrasts in both seasons and resulting lake feedbacks to the atmosphere (Fig. 7a). Prior studies have likewise confirmed that 1D lake models, when applied to deep lakes like Superior, lead to excessive ice cover, early stratification, and positive summertime LST biases (Bennington et al. 2010, 2014; Notaro et al. 2013a, 2015a,b; Xiao et al. 2016). Data users and practitioners should view climatic and limnological projections for deep lake basins with added caution when working with climate models coupled to 1D lake models. For the NoLakeMod GCMs, the HadISST2 dataset may provide inaccurately high ice cover over Lakes Superior and Huron and low ice cover over Lake Erie as boundary conditions, thereby favoring insufficient turbulent fluxes over the former deep lakes and excessive fluxes over the latter shallow lake (Figs. 12 and 13).
5) Coupling to a 1D lake model often leads to vastly underestimated wintertime overlake SH (Fig. 12a) and LH fluxes (Fig. 13a) for Lake Superior, as also noted by Notaro et al. (2021) due to excessive lake ice cover. Coupling to a 1D lake model causes an anomalously early seasonal peak in evaporation (Fig. 13), consistent with Notaro et al. (2015b). Deficient cold season evaporation from Lake Superior (Fig. 13a) leads to insufficient lake-effect snowfall in HighResMIP GCMs, particularly LakeMod (Fig. 5b, Fig. S3).

This evaluation of HighResMIP model performance over the GLB is not all bad news, as we highlight several promising results here. The improved grid spacing in these GCMs, compared to earlier generations of global modeling, leads to a better representation of key topographic features, including elevational gradients and the lakes, in support of generally reasonable spatial distributions of climatological snowfall across the region. These enhanced-resolution GCMs can capture the broadscale features of lake-effect snowfall. Although underestimated in intensity, the GCMs also capture the lakes' capacity to supply instability and heat and moisture fluxes to the lower atmosphere during the cold season in support of lake-effect precipitation, including the unique attributes of deeper versus shallower lakes in regulating lake-effect dynamics. Those HighResMIP GCMs that are coupled to 1D lake models, while flawed in their application to deep lakes, can simulate changing LST and ice cover and the implications to lake–atmosphere interactions in a changing climate.

While it is not surprising that GCMs inadequately account for important regional climate dynamics, like lake–atmosphere interactions, this study highlights the need to evaluate models at the regional scale to inform appropriate use of their information. The Great Lakes' misrepresentation in many HighResMIP GCMs as land or ocean grid cells, including the application of HadISST2 LST and ice cover for lake boundary conditions, is clearly insufficient for examining historical and future changes in lake–atmosphere interactions. Given the importance of lake–atmosphere interactions on climate dynamics in the GLB, this also suggests that CMIP models are insufficient for providing reliable future climate projections to climate adaptation planners and regional decision-makers. Regional organizations, like the Great Lakes Integrated Sciences and Assessments (GLISA), work at the boundary of climate science and decision-making to enhance communities' capacity to understand, plan for, and respond to climate impacts, both now and in the future. Groups like GLISA have learned through experience, for example, through its Great Lakes Ensemble project, to provide the best available climate information for the Great Lakes region, as end users require that models adequately simulate important regional climate processes (e.g., lake-effect snow) for the information to be interpreted as credible and thus usable in their work. To meet this need, the models must advance beyond their current representation of lake–atmosphere interactions. The present study demonstrates the need to expand beyond 1D lake models, as such simple models disregard key dynamic and thermodynamic processes of deep lakes (Xiao et al. 2016; Xue et al. 2017; Notaro et al. 2021). By coupling climate models to 3D lake models, critical lake dynamic components can be addressed, including shear instabilities, mixing episodes, Ekman suction, upwelling, downwelling, coastal currents and jets, seiches, and ice motion (Martynov et al. 2010; Bennington et al. 2010, 2014; Beletsky et al. 2012; Fujisaki et al. 2013), ideally reducing simulated biases in LST and ice cover (Notaro et al. 2013a; Xue et al. 2015, 2017; Sharma et al. 2018; Ye et al. 2019). As new simulations based on 3D lake models become available, there is the potential for an entirely new class of climate projections to better serve regional practitioners. These projections can be incorporated into a new consumer-reports-style framework to help users select models for their work (Briley et al. 2021), and perhaps

combined with more qualitative approaches like scenario planning that use quantitative information (e.g., future climate projections) to consider a range of plausible futures. In doing so, there is an opportunity to transform these models' utility to actionable information that informs management decisions across a range of sectors and timelines.

Acknowledgments. The project was funded by NOAA's Modeling, Analysis, Predictions, and Projections Program (NA18OAR4310278); GLISA (NA15OAR4310148, NA20OAR4310148A, NA21OAR4310307); NASA's Modeling, Analysis, and Prediction Program (80NSSC17K0291); and the University of Wisconsin–Madison Pandemic Affected Research Continuation Initiative and used NOAA high performance computational resources. The World Climate Research Programme is acknowledged, which, through its Working Group on Coupled Modelling, coordinated and promoted CMIP6. Appreciation is given to the modeling groups for producing and making available their output, ESGF for archiving the data and providing access, and funding agencies who support CMIP6 and ESGF. The PRIMAVERA project is acknowledged, funded by the European Union's Horizon 2020 programme under Grant Agreement 641727. Turbulent flux data were provided by GLEN, with data compilation provided by LimnoTech under Award 10042-400759 from the International Joint Commission (IJC) through a subcontract with the Great Lakes Observing System (GLOS). The statements, findings, conclusions, and recommendations are those of the authors and do not reflect the views of GLEN, LimnoTech, IJC, or GLOS.

REFERENCES

Almazroui, M., and Coauthors, 2021: Projected changes in temperature and precipitation over the United States, Central America, and the Caribbean in CMIP6 GCMs. *Earth Syst. Environ.*, **5**, 1–24, https://doi.org/10.1007/s41748-021-00199-5.

Angel, J. R., and Coauthors, 2018: Midwest. *Impacts, Risks, and Adaptation in the United States: The Fourth National Climate Assessment*, Vol. II. U.S. Global Change Research program, 872–940, https://doi.org/10.7930/NCA4.2018.CH21.

Assel, R. A., 1990: An ice-cover climatology for Lake Erie and Lake Superior for the winter seasons 1897–98 to 1982–83. *Int. J. Climatol.*, **10**, 731–748, https://doi.org/10.1002/joc.3370100707.

——, 2003: An electronic atlas of Great Lakes ice cover: Winters: 1973–2002. NOAA Great Lakes Environmental Research Laboratory, accessed 1 June 2021, http://www.glerl.noaa.gov/data/ice/atlas.

——, 2005: Great Lakes ice cover climatology update: Winters 2003, 2004, and 2005. NOAA Tech. Memo. GLERL-135, 20 pp., www.glerl.noaa.gov/pubs/tech_reports/glerl-135/tm-135.pdf.

Bador, M., and Coauthors, 2020: Impact of higher spatial atmospheric resolution on precipitation extremes over land in global climate models. *J. Geophys. Res. Atmos.*, **125**, e2019JD032184, https://doi.org/10.1029/2019JD032184.

Ballentine, R. J., A. J. Stamm, E. F. Chermack, G. P. Byrd, and D. Schleede, 1998: Mesoscale model simulation of the 4–5 January 1995 lake-effect snowstorm. *Wea. Forecasting*, **13**, 893–920, https://doi.org/10.1175/1520-0434(1998)013<0893:MMSOTJ>2.0.CO;2.

Barrett, A., 2003: National Operational Hydrologic Remote Sensing Center Snow Data Assimilation System (SNODAS) products at NSIDC. NSIDC Special Rep. 11, 19 pp., https://nsidc.org/pubs/documents/special/nsidc_special_report_11.pdf.

Barsugli, J. J., and Coauthors, 2013: The practitioner's dilemma: How to assess the credibility of downscaled climate projections. *Eos, Trans. Amer. Geophys. Union*, **94**, 424–425, https://doi.org/10.1002/2013EO460005.

Bates, G. T., F. Giorgi, and S. W. Hostetler, 1993: Toward the simulation of the effects of the Great Lakes on regional climate. *Mon. Wea. Rev.*, **121**, 1373–1387, https://doi.org/10.1175/1520-0493(1993)121<1373:TTSOTE>2.0.CO;2.

Beletsky, D., N. Hawley, Y. R. Rao, H. A. Vanderploeg, R. Beletsky, D. J. Schwab, and S. A. Ruberg, 2012: Summer thermal structure and anticyclonic circulation of Lake Erie. *Geophys. Res. Lett.*, **39**, L06605, https://doi.org/10.1029/2012GL051002.

Bennington, V., G. A. McKinley, N. Kimura, and C. H. Wu, 2010: General circulation of Lake Superior: Mean, variability, and trends from 1979 to 2006. *J. Geophys. Res.*, **115**, C12015, https://doi.org/10.1029/2010JC006261.

——, M. Notaro, and K. D. Holman, 2014: Improving climate sensitivity of deep lakes within a regional climate model and its impacts on simulated climate. *J. Climate*, **27**, 2886–2911, https://doi.org/10.1175/JCLI-D-13-00110.1.

Blanken, P. D., C. Spence, N. Hedstrom, and J. D. Lenters, 2011: Evaporation from Lake Superior: 1. Physical controls and processes. *J. Great Lakes Res.*, **37**, 707–716, https://doi.org/10.1016/j.jglr.2011.08.009.

Braham, R. R., Jr., and M. J. Dungey, 1984: Quantitative estimates of the effect of Lake Michigan on snowfall. *J. Climate Appl. Meteor.*, **23**, 940–949, https://doi.org/10.1175/1520-0450(1984)023<0940:QEOTEO>2.0.CO;2.

Briley, L. J., W. S. Ashley, R. B. Rood, and A. Krmenec, 2017: The role of meteorological processes in the description of uncertainty for climate change decision-making. *Theor. Appl. Climatol.*, **127**, 643–654, https://doi.org/10.1007/s00704-015-1652-2.

——, R. B. Rood, and M. Notaro, 2021: Large lakes in climate models: A Great Lakes case study on the usability of CMIP5. *J. Great Lakes Res.*, **47**, 405–418, https://doi.org/10.1016/j.jglr.2021.01.010.

Brown, L. C., and C. R. Duguay, 2010: The response and role of ice cover in lake-climate interactions. *Prog. Phys. Geogr.*, **34**, 671–704, https://doi.org/10.1177/0309133310375653.

Carroll, T., D. Cline, G. Fall, A. Nilsson, L. Li, and A. Rost, 2001: NOHRSC operations and the simulation of snow cover properties for the coterminous U.S. *Proc. 69th Annual Western Snow Conf.*, Sun Valley, ID, Western Snow Conference.

——, ——, C. Olheiser, A. Rost, A. Nilsson, G. Fall, C. Bovitz, and L. Li, 2006: NOAA's national snow analyses. *Proc. Western Snow Conf.*, Las Cruces, NM, Western Snow Conference, www.westernsnowconference.org/sites/westernsnowconference.org/PDFs/2006Carroll.pdf.

Changnon, S. A., Jr., 1979: How a severe winter impacts on individuals. *Bull. Amer. Meteor. Soc.*, **60**, 110–114, https://doi.org/10.1175/1520-0477(1979)060<0110:HASWIO>2.0.CO;2.

——, and D. M. A. Jones, 1972: Review of the influences of the Great Lakes on weather. *Water Resour. Res.*, **8**, 360–371, https://doi.org/10.1029/WR008i002p00360.

Clow, D. W., L. Nanus, K. L. Verdin, and J. Schmidt, 2012: Evaluation of SNODAS snow depth and snow water equivalent estimates for the Colorado Rocky Mountains, USA. *Hydrol. Processes*, **26**, 2583–2591, https://doi.org/10.1002/hyp.9385.

Colucci, S. J., 1976: Winter cyclone frequencies over the eastern United States and adjacent western Atlantic: 1964–1973. *Bull. Amer. Meteor. Soc.*, **57**, 548–553, https://doi.org/10.1175/1520-0477(1976)057<0548:WCFOTE>2.0.CO;2.

Eichenlaub, V. L., 1979: *Weather and Climate of the Great Lakes Region.* University of Notre Dame Press, 335 pp.

Fujisaki, A., J. Wang, H. Hu, D. J. Schwab, N. Hawley, and Y. R. Rao, 2013: A modeling study of ice–water processes for Lake Erie applying coupled ice-circulation models. *J. Great Lakes Res.*, **38**, 585–599, https://doi.org/10.1016/j.jglr.2012.09.021.

Gates, O., and R. Rood, 2021: In global climate model, we trust? An introduction to trusting global climate models and bias correction. GLISA White Paper, 13 pp., http://glisa.umich.edu/an-introduction-to-trusting-global-climate-models-and-bias-correction.

George, J. J., 1940: On the distortion of stream fields by small heat sources. *Mon. Wea. Rev.*, **68**, 63–66, https://doi.org/10.1175/1520-0493(1940)068<0063:OTDOSF>2.0.CO;2.

Gerbush, M. R., D. A. R. Kristovich, and N. F. Laird, 2008: Mesoscale boundary layer and heat flux variations over pack ice-covered Lake Erie. *J. Appl. Meteor. Climatol.*, **47**, 668–682, https://doi.org/10.1175/2007JAMC1479.1.

Gula, J., and W. R. Peltier, 2012: Dynamical downscaling over the Great Lakes basin of North America using the WRF regional climate model: The impact of the Great Lakes system on regional greenhouse warming. *J. Climate*, **25**, 7723–7742, https://doi.org/10.1175/JCLI-D-11-00388.1.

Haarsma, R. J., and Coauthors, 2016: High Resolution Model Intercomparison Project (HighResMIP v1.0) for CMIP6. *Geosci. Model Dev.*, **9**, 4185–4208, https://doi.org/10.5194/gmd-9-4185-2016.

Hjelmfelt, M. R., and R. R. Braham Jr., 1983: Numerical simulation of the airflow over Lake Michigan for a major lake-effect snow event. *Mon. Wea. Rev.*, **111**, 205–219, https://doi.org/10.1175/1520-0493(1983)111<0205:NSOTAO>2.0.CO;2.

Holman, K. D., A. Gronewold, M. Notaro, and A. Zarrin, 2012: Improving historical precipitation estimates over the Lake Superior basin. *Geophys. Res. Lett.*, **39**, L03405, https://doi.org/10.1029/2011GL050468.

Hostetler, S., and P. J. Bartlein, 1990: Simulation of lake evaporation with application to modeling lake-level variations at Harney-Malheur Lake, Oregon. *Water Resour. Res.*, **26**, 2603–2612, https://doi.org/10.1029/WR026i010p02603.

Kitzmiller, D., and Coauthors, 2018: The Analysis of Record for Calibration (AORC). NOAA National Weather Service Doc., 40 pp., https://hydrology.nws.noaa.gov/aorc-historic/Documents/AORC-Version1.1-SourcesMethodsandVerifications.pdf.

Kristovich, D. A. R., and N. F. Laird, 1998: Observations of widespread lake-effect cloudiness: Influences of lake surface temperature and upwind conditions. *Wea. Forecasting*, **13**, 811–821, https://doi.org/10.1175/1520-0434(1998)013<0811:OOWLEC>2.0.CO;2.

Kunkel, K. E., N. E. Westcott, and D. Kristovich, 2002: Assessment of potential effects of climate change on heavy lake-effect snowstorms near Lake Erie. *J. Great Lakes Res.*, **28**, 521–536, https://doi.org/10.1016/S0380-1330(02)70603-5.

Lemire, F., 1961: Winds on the Great Lakes. University of Toronto Great Lakes Institute Preliminary Rep. 2, 16 pp.

Lenters, J. D., J. B. Anderton, P. Blanken, C. Spence, and A. E. Suyker, 2013: Assessing the impacts of climate variability and change on Great Lakes evaporation: Implications for water levels and the need for a coordinated observation network. GLISA 2011 Project Rep., 11 pp., https://glisa.umich.edu/wp-content/uploads/2021/02/GLISA_Lake_Evaporation_Lenters_Final.pdf.

Malardel, S., N. Wedi, W. Deconinck, M. Diamantakis, C. Kuhnlein, G. Mozdzynski, M. Hamrud, and P. Smolarkiewicz, 2016: A new grid for the IFS. *ECMWF Newsletter*, No. 146, ECMWF, Reading, United Kingdom, 23–28, https://www.ecmwf.int/node/17262.

Mallard, M. S., C. G. Nolte, O. R. Bullock, T. L. Spero, and J. Gula, 2014: Using a coupled lake model with WRF for dynamical downscaling. *J. Geophys. Res. Atmos.*, **119**, 7193–7208, https://doi.org/10.1002/2014JD021785.

——, and Coauthors, 2015: Technical challenges and solutions in representing lakes when using WRF in downscaling applications. *Geosci. Model Dev.*, **8**, 1085–1096, https://doi.org/10.5194/gmd-8-1085-2015.

Martynov, A., L. Sushama, and R. Laprise, 2010: Simulation of temperate freezing lakes by one-dimensional lake models: Performance assessment for interactive coupling with regional climate models. *Boreal Environ. Res.*, **15**, 143–164.

——, ——, ——, K. Winger, and B. Dugas, 2012: Interactive lakes on the Canadian Regional Climate Model, version 5: The role of lakes in the regional climate of North America. *Tellus*, **64**, 16226, https://doi.org/10.3402/tellusa.v64i0.16226.

Minallah, S., and A. L. Steiner, 2021: Analysis of the atmospheric water cycle for the Laurentian Great Lakes region using CMIP6 models. *J. Climate*, **34**, 4693–4710, https://doi.org/10.1175/JCLI-D-20-0751.1.

Mironov, D., and Coauthors, 2010: Implementation of the lake parameterisation scheme FLake into the numerical weather prediction model COSMO. *Boreal Environ. Res.*, **15**, 218–230.

Niziol, T. A., W. R. Snyder, and J. S. Waldstreicher, 1995: Winter weather forecasting throughout the eastern United States. Part IV: Lake effect snow. *Wea. Forecasting*, **10**, 61–77, https://doi.org/10.1175/1520-0434(1995)010<0061:WWFTTE>2.0.CO;2.

Norton, D. C., and S. J. Bolsenga, 1993: Spatiotemporal trends in lake-effect and continental snowfall in the Laurentian Great Lakes, 1951–1980. *J. Climate*, **6**, 1943–1956, https://doi.org/10.1175/1520-0442(1993)006<1943:STILEA>2.0.CO;2.

Notaro, M., A. Zarrin, S. Vavrus, and V. Bennington, 2013a: Simulation of heavy lake-effect snowstorms across the Great Lakes basin by RegCM4: Synoptic climatology and variability. *Mon. Wea. Rev.*, **141**, 1990–2014, https://doi.org/10.1175/MWR-D-11-00369.1.

——, K. Holman, A. Zarrin, E. Fluck, S. Vavrus, and V. Bennington, 2013b: Influence of the Laurentian Great Lakes on regional climate. *J. Climate*, **26**, 789–804, https://doi.org/10.1175/JCLI-D-12-00140.1.

——, V. Bennington, and S. Vavrus, 2015a: Dynamically downscaled projections of lake-effect snow in the Great Lakes basin. *J. Climate*, **28**, 1661–1684, https://doi.org/10.1175/JCLI-D-14-00467.1.

——, ——, and B. Lofgren, 2015b: Dynamical downscaling-based projections of Great Lakes water levels. *J. Climate*, **28**, 9721–9745, https://doi.org/10.1175/JCLI-D-14-00847.1.

——, and Coauthors, 2021: Cold season performance of the NU-WRF regional climate model in the Great Lakes region.

J. Hydrometeor., **22**, 2423–2454, https://doi.org/10.1175/JHM-D-21-0025.1.

Perroud, M., and Coauthors, 2009: Simulation of multiannual thermal profiles in deep Lake Geneva: A comparison of one-dimensional lake models. *Limnol. Oceanogr.*, **54**, 1574–1594, https://doi.org/10.4319/lo.2009.54.5.1574.

Pettersen, C., and Coauthors, 2020: A composite analysis of snowfall modes from four winter seasons in Marquette, Michigan. *J. Appl. Meteor. Climatol.*, **59**, 103–124, https://doi.org/10.1175/JAMC-D-19-0099.1.

Petterssen, S., and P. A. Calabrese, 1959: On some weather influences due to warming of the air by the Great Lakes in winter. *J. Meteor.*, **16**, 646–652, https://doi.org/10.1175/1520-0469(1959)016<0646:OSWIDT>2.0.CO;2.

Rau, E., C. Riseng, L. Vaccaro, and J. G. Read, 2020: The dynamic Great Lakes economy: Employment trends from 2009 to 2018. Michigan Sea Grant Rep., 19 pp., https://www.michiganseagrant.org/wp-content/uploads/2020/10/MICHU-20-715-Great-Lakes-Jobs-Report-fact-sheet.pdf.

Rayner, N. A., D. E. Parker, E. B. Horton, C. K. Folland, L. V. Alexander, D. P. Rowell, E. C. Kent, and A. Kaplan, 2003: Global analyses of sea surface temperature, sea ice, and night marine air temperature since the late nineteenth century. *J. Geophys. Res.*, **108**, 4407, https://doi.org/10.1029/2002JD002670.

Roeckner, E., and Coauthors, 2003: The atmospheric general circulation model ECHAM5—Part I: Model description. Max-Planck-Instit für Meteorologie Tech. Rep. 349, 133 pp.

Schmidlin, T. W., 1993: Impacts on severe winter weather during December 1989 in the Lake Erie snowbelt. *J. Climate*, **6**, 759–767, https://doi.org/10.1175/1520-0442(1993)006<0759:IOSWWD>2.0.CO;2.</jrn>

Schwab, D. J., G. A. Leshkevich, and G. C. Muhr, 1992: Satellite measurements of surface water temperature in the Great Lakes: Great Lakes CoastWatch. *J. Great Lakes Res.*, **18**, 247–258, https://doi.org/10.1016/S0380-1330(92)71292-1.

——, ——, and ——, 1999: Automated mapping of surface water temperature in the Great Lakes. *J. Great Lakes Res.*, **25**, 468–481, https://doi.org/10.1016/S0380-1330(99)70755-0.

Scott, R. W., and F. A. Huff, 1996: Impacts of the Great Lakes on regional climate conditions. *J. Great Lakes Res.*, **22**, 845–863, https://doi.org/10.1016/S0380-1330(96)71006-7.

——, and ——, 1997: Lake effects on climatic conditions in the Great Lakes basin. Illinois State Water Survey Research Rep., 75 pp.

Sharma, A., and Coauthors, 2018: The need for an integrated land-lake-atmosphere modeling system, exemplified by North America's Great Lakes region. *Earth's Future*, **6**, 1366–1379, https://doi.org/10.1029/2018EF000870.

Sousounis, P., and J. Fritsch, 1994: Lake aggregate mesoscale disturbances. Part II: A case study of the effects on regional and synoptic scale weather systems. *Bull. Amer. Meteor. Soc.*, **75**, 1793–1811, https://doi.org/10.1175/1520-0477(1994)075<1793:LAMDPI>2.0.CO;2.

Spence, C., P. D. Blanken, N. Hedstrom, V. Fortin, and H. Wilson, 2011: Evaporation from Lake Superior: 2. Spatial distribution and variability. *J. Great Lakes Res.*, **37**, 717–724, https://doi.org/10.1016/j.jglr.2011.08.013.

——, ——, J. D. Lenters, and N. Hedstrom, 2013: The importance of spring and autumn atmospheric conditions for the evaporation regime of Lake Superior. *J. Hydrometeor.*, **14**, 1647–1658, https://doi.org/10.1175/JHM-D-12-0170.1.

Stepanenko, V. M., S. Goyette, A. Martynov, M. Perroud, X. Fang, and D. Mironov, 2010: First steps of a Lake Model Intercomparison Project: LakeMIP. *Boreal Environ. Res.*, **15**, 191–202.

Subin, Z. M., W. J. Riley, and D. Mironov, 2012: An improved lake model for climate simulations: Model structure, evaluation, and sensitivity analysis in CESM1. *J. Adv. Model. Earth Syst.*, **4**, M02001, https://doi.org/10.1029/2011MS000072.

Thornton, P. E., S. W. Running, and M. A. White, 1997: Generating surfaces of daily meteorological variables over large regions of complex terrain. *J. Hydrol.*, **190**, 214–251, https://doi.org/10.1016/S0022-1694(96)03128-9.

——, M. M. Thornton, B. W. Mayer, N. Wilhelmi, Y. Wei, R. Devarakonda, and R. B. Cook, 2014: Daymet: Daily surface weather data on a 1-km Grid for North America, version 2. ORNL DAAC, accessed 1 May 2021, https://doi.org/10.3334/ORNLDAAC/1281.

Titchner, H. A., and N. A. Rayner, 2014: The Met Office Hadley Centre sea ice and sea surface temperature data set, version 2: 1. Sea ice concentrations. *J. Geophys. Res. Atmos.*, **119**, 2864–2889, https://doi.org/10.1002/2013JD020316.

Vaccaro, L., and J. Read, 2011: Vital to our nation's economy: Great Lakes jobs report. Michigan Sea Grant Rep., 7 pp., https://www.michiganseagrant.org/wp-content/uploads/2018/10/11-203-Great-Lakes-Jobs-report.pdf.

Wang, J., X. Bai, H. Hu, A. Clites, M. Colton, and B. Lofgren, 2012: Temporal and spatial variability of Great Lakes ice cover, 1973–2010. *J. Climate*, **25**, 1318–1329, https://doi.org/10.1175/2011JCLI4066.1.

Warner, T., and N. Seaman, 1990: A real-time, mesoscale numerical weather prediction system used for research, teaching, and public service at The Pennsylvania State University. *Bull. Amer. Meteor. Soc.*, **71**, 792–805, https://doi.org/10.1175/1520-0477(1990)071<0792:ARTMNW>2.0.CO;2.

Wiley, J., and A. Mercer, 2020: An updated synoptic climatology of Lake Erie and Lake Ontario heavy lake-effect snow events. *Atmosphere*, **11**, 872, https://doi.org/10.3390/atmos11080872.

——, and ——, 2021: Synoptic climatology of lake-effect snow events off the western Great Lakes. *Climate*, **9**, 43, https://doi.org/10.3390/cli9030043.

Wuebbles, D., and Coauthors, 2019: An assessment of the impacts of climate change on the Great Lakes. Environmental Law Policy Center–Chicago Council on Global Affairs Rep., 74 pp., https://elpc.org/wp-content/uploads/2020/04/2019-ELPCPublication-Great-Lakes-Climate-Change-Report.pdf.

Xia, Y., and Coauthors, 2012: Continental-scale water and energy flux analysis and validation for the North American Land Data Assimilation System project phase 2 (NLDAS-2): 1. Intercomparison and application of model products. *J. Geophys. Res.*, **117**, D03109, https://doi.org/10.1029/2011JD016048.

Xiao, C., B. M. Lofgren, J. Wang, and P. Y. Chu, 2016: Improving the lake scheme within a coupled WRF-lake model in the Laurentian Great Lakes. *J. Adv. Model. Earth Syst.*, **8**, 1969–1985, https://doi.org/10.1002/2016MS000717.

——, ——, and ——, 2018: WRF-based assessment of the Great Lakes' impact on cold season synoptic cyclones. *Atmos. Res.*, **214**, 189–203, https://doi.org/10.1016/j.atmosres.2018.07.020.

Xue, P., D. J. Schwab, and S. Hu, 2015: An investigation of the thermal response to meteorological forcing in a hydrodynamic model of Lake Superior. *J. Geophys. Res. Oceans*, **120**, 5233–5253, https://doi.org/10.1002/2015JC010740.

——, J. S. Pal, X. Ye, J. D. Lenters, C. Huang, and P. Y. Chu, 2017: Improving the simulation of large lakes in regional climate modeling: Two-way lake-atmosphere coupling with a 3D hydrodynamic model of the Great Lakes. *J. Climate*, **30**, 1605–1627, https://doi.org/10.1175/JCLI-D-16-0225.1.

Ye, X., E. J. Anderson, P. Y. Chu, C. Huang, and P. Xue, 2019: Impact of water mixing and ice formation on the warming of Lake Superior: A model-guided mechanism study. *Limnol. Oceanogr.*, **64**, 558–574, https://doi.org/10.1002/lno.11059.

Zeng, X., M. Shaikh, Y. Dai, R. E. Dickinson, and R. Myneni, 2002: Coupling of the Common Land Model in the NCAR Community Climate Model. *J. Climate*, **15**, 1832–1854, https://doi.org/10.1175/1520-0442(2002)015<1832:COTCLM>2.0.CO;2.

Zhong, Y., M. Notaro, S. J. Vavrus, and M. J. Foster, 2016: Recent accelerated warming of the Laurentian Great Lakes: Physical drivers. *Limnol. Oceanogr.*, **61**, 1762–1786, https://doi.org/10.1002/lno.10331.